
MMD-REGULARIZED UNBALANCED OPTIMAL TRANSPORT

A PREPRINT

Piyushi Manupriya
IIT Hyderabad, INDIA.
cs18m20p100002@iith.ac.in

J. Saketha Nath
IIT Hyderabad, INDIA.
saketha@cse.iith.ac.in

Pratik Jawanpuria
Microsoft IDC, INDIA.
pratik.jawanpuria@microsoft.com

August 23, 2023

ABSTRACT

We study the unbalanced optimal transport (UOT) problem, where the marginal constraints are enforced using Maximum Mean Discrepancy (MMD) regularization. Our work is motivated by the observation that the literature on UOT is focused on regularization based on ϕ -divergence (e.g., KL divergence). Despite the popularity of MMD, its role as a regularizer in the context of UOT seems less understood. We begin by deriving a specific dual of MMD-regularized UOT (MMD-UOT), which helps us prove other useful properties. One interesting outcome of this duality result is that MMD-UOT induces novel metrics, which not only lift the ground metric like the Wasserstein but are also sample-wise efficient to estimate like the MMD. Further, we present finite-dimensional convex programs for estimating MMD-UOT and the corresponding barycenter solely based on the samples from the measures being transported. Under mild conditions, we prove that our convex-program-based estimators are consistent and the estimation error decays at a rate $\mathcal{O}\left(m^{-\frac{1}{2}}\right)$, where m is the number of samples. As far as we know, such error bounds that are free from the curse of dimensionality are not known for ϕ -divergence regularized UOT. Finally, we discuss how the proposed convex programs can be solved efficiently using accelerated projected gradient descent. Our experiments show that MMD-UOT consistently outperforms popular baselines, including KL-regularized UOT and MMD, in diverse machine learning applications.

1 Introduction

Optimal transport (OT) is a popular tool for comparing probability measures while incorporating geometry over their support. OT has witnessed a lot of success in machine learning applications [53], where distributions play a central role. The Kantorovich’s formulation for OT aims to find an optimal plan for the transport of mass between the source and the target distributions that incurs the least expected cost of transportation. While classical OT strictly enforces the marginals of the transport plan to be the source and target, one would want to relax this constraint when the measures are noisy [25] or when the source and target are un-normalized [14, 40]. Unbalanced optimal transport (UOT) [14], a variant of OT, is employed in such cases, which performs a regularization-based soft-matching of the transport plan’s marginals with the source and the target distributions.

Unbalanced optimal transport with Kullback Leibler (KL) divergence and, in general, with ϕ -divergence [18] based regularization is well-explored in literature [39, 40, 14, 13, 15]. UOT with KL divergence has been explored in applications such as domain adaptation [23], natural language processing [12, 3], and computational biology [44], to name a few. Total variation (TV)-regularization-based UOT formulations have also been studied in the literature [55, 56, 32, 27], though TV-regularized UOT lacks solvers that scale to large-scale applications. Interestingly, TV distance is the only common member of the ϕ -divergence family and its complementary family of integral probability metrics (IPMs) [65]. It should be noted that IPM includes other distances as well, such as the Maximum Mean Discrepancy (MMD) [46]. While MMD-based methods have been popularly employed in several machine learning (ML) applications [30, 37, 38, 51], the applicability of MMD-based regularization for UOT is not well-understood. To the best of our knowledge, interesting questions like i) will MMD regularization also lead to novel metrics analogous to the Gaussian Hellinger-Kantorovich and Generalized Wasserstein metrics? ii) what will be the statistical estimation properties of these? iii) how can such

MMD regularized metrics be estimated in practice such that they scale to ML applications?, are not addressed in existing works. In order to bridge this gap, we study MMD-based regularization for matching the marginals of the transport plan in the UOT formulation (henceforth termed MMD-UOT).

We first derive a specific dual of the MMD-UOT formulation (Theorem 4.1), which helps further analyze its properties. One interesting consequence of this duality result is that the optimal objective of MMD-UOT is a valid distance between the source and target measures (Corollary 4.2), whenever the transport cost is valid (ground) metric over the data points. Popularly, this is known as the phenomenon of lifting metrics to measures. This result is significant as it shows that MMD-regularization in UOT can parallel the metricity-preservation that happens with KL-regularization [40] and TV-regularization [55]. Furthermore, our duality result shows that this induced metric is a novel metric belonging to the family of IPMs. Also, the generating set of this metric happens to be the intersection of the generating sets of MMD and the Kantorovich-Wasserstein metric. Because of this important relation, the proposed distance is always smaller than the MMD distance, and hence estimating MMD-UOT from samples is at least as efficient as that with MMD (Corollary 4.6). This is interesting as minimax estimation rates for MMD can be completely dimension-free. As far as we know, there are no such results that show that estimation with KL/TV-regularized UOT can be as efficient sample-wise.

Although the sample-based estimation of MMD-UOT satisfies the above-mentioned attractive convergence property, its computation involves optimization over all possible joint measures. This may be challenging¹, especially when the measures are continuous. Hence, we present a convex program-based estimator, which only involves a search over joints supported at the samples. We prove that the proposed estimator is statistically consistent and converges to MMD-UOT between the true measures at a rate $\mathcal{O}\left(m^{-\frac{1}{2}}\right)$, where m is the number of samples. Such efficient estimators are particularly useful in machine learning applications, where only samples from the underlying measures are typically available. In contrast, the minimax estimation rate for the Wasserstein distance is itself $\mathcal{O}\left(m^{-\frac{1}{d}}\right)$, where d is the dimensionality of the samples [52]. That is, even if search over all possible joints is performed, estimating Wasserstein may be challenging. Since MMD-UOT can approximate Wasserstein arbitrarily closely (as regularization hyperparameter goes ∞), our result can also be understood as a way of alleviating the curse of dimensionality problem in Wasserstein (via MMD regularization). We summarize the comparison between MMD-UOT and relevant baselines in Table 1.

Finally, our result of MMD-UOT being a metric facilitates its application whenever the metric properties of OT are desired, for example, while computing the barycenter-based interpolation for single-cell RNA sequencing [68]. Accordingly, we also present a finite-dimensional convex-program-based estimator for the barycenter with MMD-UOT. We prove that this estimator is also consistent with an efficient sample complexity. We discuss how the formulations for estimating MMD-UOT (and barycenter) can be solved efficiently using accelerated (projected) gradient descent. This solver helps us scale well to benchmark machine learning applications. We empirically show the utility of MMD-UOT in a diverse set of applications, including two-sample hypothesis testing, single-cell RNA sequencing, domain adaptation, and prompt learning for few-shot classification. In particular, we observe that MMD-UOT outperforms popular baselines, including KL-regularized UOT and MMD, in diverse machine learning applications.

We reiterate our main contributions below:

- Derivation of a dual of MMD-UOT and its analysis. We prove that MMD-UOT induces novel metrics that not only lift ground metrics like the Wasserstein but also are efficient to estimate like the MMD.
- Finite-dimensional convex-program-based estimators for MMD-UOT and the corresponding barycenter. We prove that the estimators are both statistically and computationally efficient.
- We conduct various machine learning experiments to evaluate MMD-UOT and the corresponding barycenter. The results show that the proposed approach consistently outperforms the popular baselines, showing its utility.

We present proofs for all our theory results in Appendix B. As a side-point, we note that most of our results not only hold for MMD-UOT, but also for a UOT formulation where MMD is replaced by a general IPM. Proofs in the appendix are hence written for general IPM-based regularization and then specialized to the case when the IPM is MMD. This generalization to IPMs may itself be of interest elsewhere.

¹Note that even OT and its popular variants involve the same challenge. So the challenge does not arise because of our MMD regularization and is inherent to OT.

Table 1: Summary of relevant baselines. ϵ OT and ϵ KL-UOT denote entropy-regularized OT [19] and KL-regularized UOT [14] methods, respectively, for which scalable solvers are known. MMD and MMD-UOT are shown with characteristic kernels.

Property	MMD	OT	ϵ OT	TV-UOT	KL-UOT	ϵ KL-UOT	MMD-UOT
Metricity	✓	✓	✗	✓	✓	✗	✓
Adaptive geometry	✗	✓	✓	✓	✓	✓	✓
No curse of dimensionality	✓	✗	✗	✗	✗	✗	✓

2 Preliminaries

Notations. Let \mathcal{X} be a set (domain) that forms a compact Hausdorff space. Let $\mathcal{R}^+(\mathcal{X}), \mathcal{R}(\mathcal{X})$ denote the set of all non-negative, signed (finite) Radon measures defined over \mathcal{X} ; while the set of all probability measures is denoted by $\mathcal{R}_1^+(\mathcal{X})$. For a measure on the product space, $\pi \in \mathcal{R}^+(\mathcal{X} \times \mathcal{X})$, let π_1, π_2 denote the first and second marginals, respectively (i.e., they are the push-forwards under the canonical projection maps onto \mathcal{X}). Let $\mathcal{L}(\mathcal{X}), \mathcal{C}(\mathcal{X})$ denote the set of all real-valued measurable functions and all real-valued continuous functions, respectively, over \mathcal{X} .

Integral Probability Metric (IPM): Given a set $\mathcal{G} \subset \mathcal{L}(\mathcal{X})$, the integral probability metric (IPM) [46, 66, 1] associated with \mathcal{G} , is defined by:

$$\gamma_{\mathcal{G}}(s_0, t_0) \equiv \max_{f \in \mathcal{G}} \left| \int_{\mathcal{X}} f \, ds_0 - \int_{\mathcal{X}} f \, dt_0 \right| \quad \forall s_0, t_0 \in \mathcal{R}^+(\mathcal{X}). \quad (1)$$

\mathcal{G} is called the generating set of the IPM, $\gamma_{\mathcal{G}}$.

Maximum Mean Discrepancy (MMD) Let k be a characteristic kernel [67] over the domain \mathcal{X} , let $\|f\|$ denote the norm of f in the canonical reproducing kernel Hilbert space (RKHS), \mathcal{H}_k , corresponding to k . MMD_k is the IPM associated with the generating set: $\mathcal{G}_k \equiv \{f \in \mathcal{H}_k \mid \|f\| \leq 1\}$. For the convenience of notation, we will denote it by MMD and will specify the underlying kernel wherever needed. Using a characteristic kernel k , MMD metric between $s_0, t_0 \in \mathcal{R}^+(\mathcal{X})$ is defined as:

$$\begin{aligned} \text{MMD}(s_0, t_0) &\equiv \max_{f \in \mathcal{G}_k} \left| \int_{\mathcal{X}} f \, ds_0 - \int_{\mathcal{X}} f \, dt_0 \right| \\ &= \|\mu_k(s_0) - \mu_k(t_0)\|, \end{aligned} \quad (2)$$

where $\mu_k(s) \equiv \int \phi_k(x) \, ds(x)$, is the kernel mean embedding of s [45], ϕ_k is the canonical feature map of k . MMD can be computed analytically using evaluations of the kernel k .

Optimal Transport (OT) Optimal transport provides a tool to compare distributions while incorporating the underlying geometry of their support points. Given a cost function, $c : \mathcal{X} \times \mathcal{X} \mapsto \mathbb{R}$, and two probability measures $s_0 \in \mathcal{R}_1^+(\mathcal{X}), t_0 \in \mathcal{R}_1^+(\mathcal{X})$, the p -Wasserstein Kantorovich OT formulation is given by:

$$\bar{W}_p^p(s_0, t_0) \equiv \min_{\pi \in \mathcal{R}_1^+(\mathcal{X} \times \mathcal{X})} \int c^p \, d\pi, \text{ s.t. } \pi_1 = s_0, \pi_2 = t_0, \quad (3)$$

where $p \geq 1$. An optimal solution of (3) is called an optimal transport plan. Whenever the cost is a metric, d , over $\mathcal{X} \times \mathcal{X}$ (ground metric), \bar{W}_p defines a metric over measures, known as the p -Wasserstein metric, over $\mathcal{R}_1^+(\mathcal{X}) \times \mathcal{R}_1^+(\mathcal{X})$.

Kantorovich metric (\mathcal{K}_c) Kantorovich metric also belongs to the family of integral probability metrics associated with the generating set $\mathcal{W}_c \equiv \left\{ f : \mathcal{X} \mapsto \mathbb{R} \mid \max_{x \in \mathcal{X} \neq y \in \mathcal{X}} \frac{|f(x) - f(y)|}{c(x, y)} \leq 1 \right\}$, where c is a metric over $\mathcal{X} \times \mathcal{X}$.

3 Related Work

Given the source and target measures, $s_0 \in \mathcal{R}^+(\mathcal{X})$ and $t_0 \in \mathcal{R}^+(\mathcal{X})$, respectively, the unbalanced optimal transport (UOT) approach [40, 13] aims to learn the transport plan by replacing the mass conservation marginal constraints (enforced strictly in ‘balanced’ OT setting) by a soft regularization/penalization on the marginals. KL-divergence and, in general, ϕ -divergence [18], [66] based regularizations have been most popularly studied in UOT setting. The ϕ -divergence regularized UOT formulation may be written as [25], [14]:

$$\min_{\pi \in \mathcal{R}^+(\mathcal{X} \times \mathcal{X})} \int c \, d\pi + \lambda D_{\phi}(\pi_1, s_0) + \lambda D_{\phi}(\pi_2, t_0), \quad (4)$$

where c is the ground cost metric and $D_\phi(\cdot, \cdot)$ denotes the ϕ -divergence [18, 66] between two measures.

UOT with KL-divergence based regularization induces the so-called Gaussian Hellinger-Kantorovich metric [40] between the measures whenever $0 < \lambda \leq 1$ and the ground cost c is the squared-Euclidean distance. Total Variation (TV) distance is another popular metric between measures and is the only common member of the ϕ -divergence family and the IPM family. UOT formulation with TV regularization (denoted by $|\cdot|_{\text{TV}}$) has been studied in [55]:

$$\min_{\pi \in \mathcal{R}^+(\mathcal{X} \times \mathcal{X})} \int c \, d\pi + \lambda |\pi_1 - s_0|_{\text{TV}} + \lambda |\pi_2 - t_0|_{\text{TV}}. \quad (5)$$

UOT with TV-divergence based regularization induces the so-called Generalized Wasserstein metric [55] between the measures whenever $0 < \lambda$ and the ground cost c is a valid metric.

Complementary to the family of ϕ -divergences is the family of integral probability metrics for comparing measures. An important member of the IPM family is the MMD metric which also incorporates the geometry over supports through the underlying kernel. Due to its attractive statistical properties [29], MMD has been successfully applied in a diverse set of applications in machine learning, including hypothesis testing [30], generative modelling [37], self-supervised learning [38], and reinforcement learning [51].

Recently, [47] explored learning the transport plan's kernel mean embeddings in balanced OT setup. They proposed learning the kernel mean embedding of a joint distribution with the least expected cost and whose marginal embeddings are close to the given-sample-based estimates of the marginal embeddings. As kernel mean embedding induces MMD distance, MMD-based regularization features in the balanced OT formulation of [47] as a means to control overfitting. To ensure that valid conditional embeddings are obtained from the learned joint embeddings, [47] required additional feasibility constraints which restrict their solvers in scaling well to machine learning applications. In contrast, we bypass the issues related to the validity of conditional embeddings as our formulation involves directly learning the transport plan and avoids kernel mean embedding of the transport plan. More importantly, [47] do not study the same formulation as ours. They neither discuss the dual of their formulation nor show the metric-related properties and perform lesser empirical evaluation than us. We perform a detailed study of MMD regularization for UOT, which includes deriving the dual and proving metric properties that are crucial for OT formulations. To the best of our knowledge, the metricity of MMD-regularized UOT formulations has not been studied previously. Also, as the formulations themselves are different, the sample complexity result of $\mathcal{O}(m^{-\frac{1}{2}})$ in [47] does not apply to our MMD-UOT estimator. While we also obtain the $\mathcal{O}(m^{-\frac{1}{2}})$ estimation error rate, we require a different proof strategy. Finally, as discussed in Appendix B, most of our theoretical contributions apply to a general IPM-regularized UOT formulation and are not limited to an MMD-regularized formulation like in [47].

4 MMD Regularization for UOT

We propose to study the following UOT formulation where the marginal constraints are enforced using MMD regularization.

$$\begin{aligned} \mathcal{U}_{k,c,\lambda_1,\lambda_2}(s_0, t_0) &\equiv \min_{\pi \in \mathcal{R}^+(\mathcal{X} \times \mathcal{X})} \int c \, d\pi + \lambda_1 \text{MMD}(\pi_1, s_0) + \lambda_2 \text{MMD}(\pi_2, t_0) \\ &= \min_{\pi \in \mathcal{R}^+(\mathcal{X} \times \mathcal{X})} \int c \, d\pi + \lambda_1 \|\mu_k(\pi_1) - \mu_k(s_0)\| + \lambda_2 \|\mu_k(\pi_2) - \mu_k(t_0)\|, \end{aligned} \quad (6)$$

where $\mu_k(s)$ is the kernel mean embedding of s (defined in Section 2) induced by the characteristic kernel k used in the generating set $\mathcal{G}_k \equiv \{f \in \mathcal{H}_k \mid \|f\| \leq 1\}$, and $\lambda_1, \lambda_2 > 0$ are the regularization hyper-parameters.

We begin by presenting a key duality result.

Theorem 4.1. (Duality) *Whenever c is a (continuous) ground metric over compact $\mathcal{X} \times \mathcal{X}$, and $\lambda_1 = \lambda_2 = \lambda$, we have that:*

$$\mathcal{U}_{k,c,\lambda,\lambda}(s_0, t_0) = \max_{f \in \mathcal{G}_k(\lambda) \cap \mathcal{W}_c} \int_{\mathcal{X}} f \, ds_0 - \int_{\mathcal{X}} f \, dt_0. \quad (7)$$

Here, $\mathcal{G}_k(\lambda) \equiv \{g \in \mathcal{H}_k \mid \|g\| \leq \lambda\}$ and \mathcal{W}_c is the set of all 1-Lipschitz functions wrt. metric c .

The duality result helps us to study several properties of the MMD-UOT formulation (6), discussed below. The proof of the Theorem 4.1 is provided in Appendix B.1.

Applications in machine learning often deal with comparing distributions and employ optimal transport as a metric over distributions. While prior works have shown metric properties of KL-regularized UOT [40] and TV-regularized UOT [56], it is an open question if MMD-regularization in UOT can also lead to valid metrics. The following result answers this affirmatively.

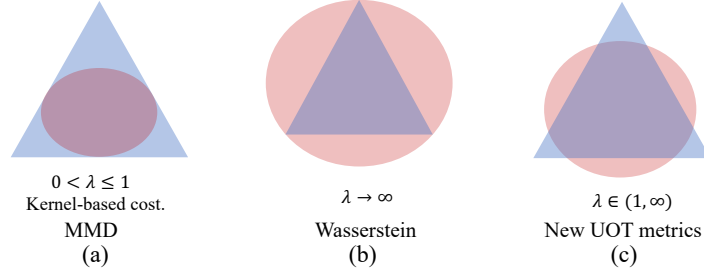


Figure 1: (Best viewed in color) For illustration, the generating set of Kantorovich-Wasserstein is depicted as a triangle, and the scaled generating set of MMD is depicted as a disc. The intersection represents the generating set of the IPM metric induced by MMD-UOT. Fig. (a) shows the special case when our MMD-UOT metric recovers back the sample-efficient MMD metric, Fig. (b) shows the special case when our MMD-UOT metric reduces to the Kantorovich-Wasserstein metric incorporating geometry over supports, and Fig. (c) results in a family of new UOT metrics which have both sample-efficiency and incorporates the geometry over supports.

Corollary 4.2. (Metricity) *Whenever c is a (continuous) ground metric, $\mathcal{U}_{k,c,\lambda,\lambda}$ belongs to the family of integral probability metrics (IPMs) where the generating set is the intersection of the generating set of the Kantorovich metric and scaled-version of the generating set of the MMD used for regularization. Further, $\mathcal{U}_{k,c,\lambda,\lambda}$ is a valid norm-induced metric over measures whenever k is characteristic.*

We present the proof of Corollary 4.2 in Appendix B.2. This result also reveals interesting relationships between $\mathcal{U}_{k,c,\lambda,\lambda}$, the Kantorovich metric, \mathcal{K}_c , and the MMD metric used for regularization. This is summarized in the following two results.

Corollary 4.3. (Interpolant) *We have that $\forall s_0, t_0 \in \mathcal{R}^+(\mathcal{X})$, $\lim_{\lambda \rightarrow \infty} \mathcal{U}_{k,c,\lambda,\lambda}(s_0, t_0) = \mathcal{K}_c(s_0, t_0)$. Further, when the cost metric, c , dominates the kernel, k , induced metric, i.e., $c(x, y) \geq \sqrt{k(x, x) + k(y, y) - 2k(x, y)} \forall x, y \in \mathcal{X}$, then $\mathcal{U}_{k,c,\lambda,\lambda}(s_0, t_0) = \lambda \text{MMD}(s_0, t_0)$ whenever $0 < \lambda \leq 1$. In particular, for such a dominating cost, c , the metric induced by MMD-UOT interpolates between the scaled MMD and Kantorovich-Wasserstein as λ moves between $[1, \infty)$. The nature of this interpolation is already described in terms of generating sets in Corollary 4.2.*

We illustrate this interpolation result in Figure 1. Our proof of Corollary 4.3, presented in Appendix B.3, also shows that the Euclidean distance satisfies such a dominating cost assumption when the kernel employed is the Gaussian kernel and the inputs lie on a unit-norm ball. The next result presents another relationship between the metrics in the discussion.

Corollary 4.4. $\mathcal{U}_{k,c,\lambda,\lambda}(s, t) \leq \min(\lambda \text{MMD}(s, t), \mathcal{K}_c(s, t))$.

We discuss the proof of Corollary 4.4 in Appendix B.5. This simple yet important result enables us to show properties like weak metrization and sample efficiency with MMD-UOT. For a sequence $s_n \in \mathcal{R}_1^+(\mathcal{X})$, $n \geq 1$, we say that s_n weakly converges to $s \in \mathcal{R}_1^+(\mathcal{X})$ (denoted as $s_n \rightharpoonup s$), if and only if $\mathbb{E}_{X \sim s_n}[f(X)] \rightarrow \mathbb{E}_{X \sim s}[f(X)]$ for all bounded continuous functions over \mathcal{X} . It is natural to ask when is the convergence in metric over measures equivalent to weak convergence on measures. The metric is then said to metrize the weak convergence of measures or is equivalently said to weak metrize on measures. The weak metrization properties of the Wasserstein metric and MMD are well-understood (e.g., refer Theorem 6.9 in [69] and Theorem 7 in [60]). The weak metrization property of $\mathcal{U}_{k,c,\lambda,\lambda}$ follows from the above Corollary 4.4.

Corollary 4.5. (Weak Metrization) $\mathcal{U}_{k,c,\lambda,\lambda}$ metrizes the weak convergence of normalized measures.

The proof is presented in Appendix B.6. We now show that the metric induced by MMD-UOT inherits the attractive statistical efficiency of the MMD metric. In typical machine learning applications, only finite samples are given from the measures. Hence, it is important to study statistically efficient metrics that alleviate the curse of dimensionality problem prevalent in OT [52]. Sample complexity result with the metric induced by MMD-UOT is presented as follows.

Corollary 4.6. (Sample Complexity) *Let us denote $\mathcal{U}_{k,c,\lambda,\lambda}$, defined in (6), by $\bar{\mathcal{U}}$. Let \hat{s}_m, \hat{t}_m denote the empirical estimates of $s_0, t_0 \in \mathcal{R}^+(\mathcal{X})$ respectively with m samples. Then, $\bar{\mathcal{U}}(\hat{s}_m, \hat{t}_m) \rightarrow \bar{\mathcal{U}}(s_0, t_0)$ at a rate (apart from constants) same as that of $\text{MMD}(\hat{s}_m, s_0) \rightarrow 0$.*

Since the sample complexity of MMD with a normalized characteristic kernel is $\mathcal{O}(m^{-\frac{1}{2}})$ [61], the same will be the complexity for the corresponding MMD-UOT. The proof of Corollary 4.6 is presented in Appendix B.7. This

is interesting because, though MMD-UOT can arbitrarily well approximate Wasserstein (as $\lambda \rightarrow \infty$), its estimation can be far more efficient than $\mathcal{O}\left(m^{-\frac{1}{d}}\right)$, which is the minimax estimation rate for the Wasserstein. Here, d is the dimensionality of the samples [52]. In Appendix S.4, we show that even when MMD^q ($q > 1 \in \mathbb{Z}$) is used for regularization, the sample complexity again comes out to be $\mathcal{O}\left(m^{-\frac{1}{2}}\right)$.

Another desirable property of a metric is robustness to noise. We consider the same noise model as the one considered for studying the robustness of KL-regularized UOT [23, Lemma 1]. The robustness property of the MMD-UOT formulation is presented below.

Lemma 4.7. (Robustness) *Let $s_0, t_0 \in \mathcal{R}_1^+(\mathcal{X})$. Consider $s_c = \rho s_0 + (1 - \rho)\delta_z$ ($\rho \in [0, 1]$), a distribution perturbed by a Dirac outlier located at some z outside of the support of t_0 . Let $m(z) = \int c(z, y) dt_0(y)$. We have that, $\mathcal{U}_{k,c,\lambda_1,\lambda_2}(s_c, t_0) \leq \rho \mathcal{U}_{k,c,\lambda_1,\lambda_2}(s_0, t_0) + (1 - \rho)m(z)$.*

The proof is presented in Appendix B.8.

Remark 4.8. *Interestingly, most of our theory results not only hold with the MMD-UOT Formulation (8) but also with a general IPM-regularized UOT formulation which we discuss in Appendix B. This generalization may be of independent interest for future work.*

4.1 Finite-Sample-based Estimation

As noted in Corollary 4.6, MMD-UOT can be efficiently estimated from samples of source and target. However, when the measures have densities (continuous random variable), one needs to solve an optimization problem over all possible joint (un-normalized) densities. This can be computationally expensive. Hence, in this section, we propose a simple estimator where the optimization is only over the joint measures supported at sample-based points. We show that our estimator is consistent and can be computed efficiently.

Let m samples be given from the source, target, $s_0, t_0 \in \mathcal{R}^+(\mathcal{X})$ respectively. We denote $\mathcal{D}_i = \{x_{i1}, \dots, x_{im}\}$, $i = 1, 2$ as the set of samples given from s_0, t_0 respectively. Let \hat{s}_m, \hat{t}_m denote the empirical measures using samples $\mathcal{D}_1, \mathcal{D}_2$. Let us denote the Gram-matrix of \mathcal{D}_i by G_{ii} . Let \mathcal{C}_{12} be the $m \times m$ cost matrix with entries as evaluations of the cost function over $\mathcal{D}_1 \times \mathcal{D}_2$. Following the common practice in OT literature [15, 19, 21, 23, 35, 4, 47, 53], we restrict the transport plan to be supported on the finite samples from each of the measures in order to avoid the computational issues in optimizing over all possible joint densities. More specifically, let α be the $m \times m$ (parameter/variable) matrix with entries as $\alpha_{ij} \equiv \pi(x_{1i}, x_{2j})$ where $i, j \in \{1, \dots, m\}$. With these notations and the mentioned restricted feasibility set, Problem (6) simplifies to the following, denoted by $\hat{\mathcal{U}}_m(\hat{s}_m, \hat{t}_m)$:

$$\min_{\alpha \geq 0 \in \mathbb{R}^{m \times m}} \text{Tr}(\alpha \mathcal{C}_{12}^\top) + \lambda_1 \left\| \alpha \mathbf{1} - \frac{\sigma_1}{m} \mathbf{1} \right\|_{G_{11}} + \lambda_2 \left\| \alpha^\top \mathbf{1} - \frac{\sigma_2}{m} \mathbf{1} \right\|_{G_{22}}, \quad (8)$$

where $\text{Tr}(M)$ denotes the trace of matrix M , $\|x\|_M \equiv \sqrt{x^\top M x}$, and σ_1, σ_2 are the masses of the source, target measures, s_0, t_0 , respectively.

As the transport plan is supported on the given finite samples, it is important to study the estimation error as a function of the number of samples. The following result shows that our sample-based estimator (8) is consistent, and the estimation error decays at a favourable rate.

Theorem 4.9. (Consistency of the proposed estimator) *Let us denote $\mathcal{U}_{k,c,\lambda_1,\lambda_2}$, defined in (6), by $\bar{\mathcal{U}}$. Let π^* be the optimal transport plan between s_0 and t_0 , obtained with $\bar{\mathcal{U}}$. Let $\eta(x, y) \equiv \frac{\pi^*(x, y)}{s_0(x)t_0(y)}$, $\eta_1(x) \equiv \frac{\pi_1^*(x)}{s_0(x)}$ and $\eta_2(x) \equiv \frac{\pi_2^*(x)}{t_0(y)}$. Under the mild assumption that the functions, η, η_1, η_2 and $c \in \mathcal{H}_k$, we have that w.h.p., the estimation error, $\left| \hat{\mathcal{U}}_m(\hat{s}_m, \hat{t}_m) - \bar{\mathcal{U}}(s_0, t_0) \right| \leq \mathcal{O}(m^{-\frac{1}{2}})$.*

We discuss the proof of the above theorem in Appendix B.12.

4.2 Computational Aspects

Problem (8) is an instance of a convex program and can be solved using mirror descent algorithm given in 2.

Following standard arguments (detailed in Appendix B.11), consider the following equivalent formulation, which helps us to exploit faster solvers for MMD-UOT:

$$\min_{\alpha \geq 0 \in \mathbb{R}^{m \times m}} \text{Tr}(\alpha \mathcal{C}_{12}^\top) + \lambda_1 \left\| \alpha \mathbf{1} - \frac{\sigma_1}{m} \mathbf{1} \right\|_{G_{11}}^2 + \lambda_2 \left\| \alpha^\top \mathbf{1} - \frac{\sigma_2}{m} \mathbf{1} \right\|_{G_{22}}^2. \quad (9)$$

Algorithm 1 Accelerated Projected Gradient Descent for solving Problem (9).**Require:** Lipschitz constant L , initial $\alpha_0 \in \mathbb{R}^{m \times m} \geq 0$.

$$f(\alpha) = \text{Tr}(\alpha \mathcal{C}_{12}^\top) + \lambda_1 \left\| \alpha \mathbf{1} - \frac{\sigma_1}{m} \mathbf{1} \right\|_{G_{11}}^2 + \lambda_2 \left\| \alpha^\top \mathbf{1} - \frac{\sigma_2}{m} \mathbf{1} \right\|_{G_{22}}^2.$$

$$\gamma_1 = 1.$$

$$y_1 = \alpha_0.$$

while not converged **do**

$$\alpha_i = \text{Project}_{\geq 0} \left(y_i - \frac{1}{L} \nabla f(y_i) \right).$$

$$\gamma_{i+1} = \frac{1 + \sqrt{1 + 4\gamma_i^2}}{2}.$$

$$y_{i+1} = \alpha_i + \frac{\gamma_i - 1}{\gamma_{i+1}} (\alpha_i - \alpha_{i-1}).$$

end while**return** α_i .

We show that the gradient of the objective in Problem (9) is L -smooth, which enables us to use the accelerated projected gradient descent (APGD) algorithm [49, 48, 5] with fixed step-size $\tau = 1/L$ for solving Problem (9), presented in Algorithm 1. The below result (proof detailed in Appendix B.13) gives an expression of the smoothness constant for Problem (9).

Lemma 4.10. *The gradient of the objective in Problem(9) is L -smooth with,*

$$L = 2\sqrt{(\lambda_1 m)^2 \|G_{11}\|_F^2 + (\lambda_2 m)^2 \|G_{22}\|_F^2 + 2\lambda_1 \lambda_2 (\mathbf{1}_m^\top (G_{11} + G_{22}) \mathbf{1}_m)}.$$

The overall computation cost for solving MMD-UOT (9) is $\mathcal{O}(\frac{m^2}{\sqrt{\epsilon}})$ where ϵ is the optimality gap. In Appendix C.1, we compare the computation time taken to solve MMD-UOT formulation (9) using APGD algorithm against the computation time to solve ϵ KL-UOT using the popular Sinkhorn algorithm [19, 15, 54]. We observe that the APGD-based solver for MMD-UOT is indeed computationally efficient.

4.3 Barycenter

A related problem is that of barycenter interpolation of measures [2], which has interesting applications [63, 62, 28]. Given measures s_1, \dots, s_n with total masses $\sigma_1, \dots, \sigma_n$ respectively, and interpolation weights ρ_1, \dots, ρ_n , the barycenter $s \in \mathcal{R}^+(\mathcal{X})$ is defined as the solution of $\hat{\mathcal{B}}(s_1, \dots, s_n) \equiv \min_{s \in \mathcal{R}^+(\mathcal{X})} \sum_{i=1}^n \rho_i \mathcal{U}_{k,c,\lambda_1,\lambda_2}(s_i, s)$.

In typical applications, only sample sets, \mathcal{D}_i , from s_i are available instead of s_i themselves. Let us denote the corresponding empirical measures by $\hat{s}_1, \dots, \hat{s}_n$. One way to estimate the barycenter is to consider $\hat{\mathcal{B}}(\hat{s}_1, \dots, \hat{s}_n)$. However, this may be challenging to solve computationally whenever the measures involved are continuous. So we propose estimating the barycenter with the restriction that the transport plan π^i corresponding to $\mathcal{U}_{k,c,\lambda_1,\lambda_2}(\hat{s}_i, s)$ is supported on $\mathcal{D}_i \times \cup_{i=1}^n \mathcal{D}_i$. And, let $\alpha_i \geq 0 \in \mathbb{R}^{m_i \times m}$ denote the corresponding probabilities. Let us denote the barycenter problem with this restriction on the transport plans as $\hat{\mathcal{B}}_m(\hat{s}_1, \dots, \hat{s}_n)$. Let G be the Gram-matrix of $\cup_{i=1}^n \mathcal{D}_i$ and C_i be the $m_i \times m$ matrix with entries as evaluations of the cost function.

Lemma 4.11. *The barycenter problem $\hat{\mathcal{B}}_m(\hat{s}_1, \dots, \hat{s}_n)$ can be equivalently written as:*

$$\min_{\alpha_1, \dots, \alpha_n \geq 0} \sum_{i=1}^n \rho_i \left(\text{Tr}(\alpha_i C_i^\top) + \lambda_1 \left\| \alpha_i \mathbf{1} - \frac{\sigma_i}{m_i} \mathbf{1} \right\|_{G_{ii}}^2 + \lambda_2 \left\| \alpha_i^\top \mathbf{1} - \sum_{j=1}^n \rho_j \alpha_j^\top \mathbf{1} \right\|_G^2 \right). \quad (10)$$

We present the proof in Appendix B.15.1. Similar to Problem (9), the objective in Problem (10) is a smooth quadratic program in each α_i and is jointly convex in α_i 's. In Appendix B.15.2, we also present the details for solving Problem (10) using APGD as well as its statistical consistency.

5 Experiments

5.1 Two-Sample Hypothesis Test

Given two sets of samples $\{x_1, \dots, x_m\} \sim s_0$ and $\{y_1, \dots, y_m\} \sim t_0$, the two-sample test aims to determine whether the two sets of samples are drawn from the same distributions, viz., to predict if $s_0 = t_0$. The performance evaluation in the two-sample test relies on two types of errors. Type-I error occurs when $s_0 = t_0$ but the algorithm predicts otherwise.

Table 2: Average Test Power (between 0 and 1; higher is better) on MNIST. MMD-UOT obtains the highest average test power at all timesteps.

N	MMD	ϵ KL-UOT	MMD-UOT
100	0.137	0.099	0.154
200	0.258	0.197	0.333
300	0.467	0.242	0.588
400	0.656	0.324	0.762
500	0.792	0.357	0.873
1000	0.909	0.506	0.909

Type-II error occurs when the algorithm incorrectly predicts $s_0 = t_0$. The probability of Type-I error is called the significance level. The significance level can be controlled using permutation test-based setups [22, 41]. Algorithms are typically compared based on the empirical estimate of their test power (higher is better), which is defined as the probability of not making a Type-II error and the average Type-I error (lower is better).

Dataset and experimental setup. Following [41], we consider the two sets of samples, one from the true MNIST [36] and another from fake MNIST generated by the DCGAN [7]. The data lies in 1024 dimensions. We take an increasing number of samples (N) and compute the average test power over 100 pairs of sets for each value of N . We repeat the experiment 10 times and report the average test power in Table 2 for the significance level $\alpha = 0.05$. By the design of the test, the average Type-I error was upper-bounded, and we noted the Type-II error in our experiment. We detail the procedure for choosing the hyperparameters and the list of chosen hyperparameters for each method in Appendix C.2.

Results. In Table 2, we observe that MMD-UOT obtains the highest test power for all values of N . The average test power of MMD-UOT is 1.5 – 2.4 times better than that of ϵ KL-UOT across N . MMD-UOT also outperforms EMD and 2-Wasserstein, which suffer from the curse of dimensionality, for all values of N . Our results match the sample efficient MMD metric’s result on increasing N to 1000, but for lesser sample-size, MMD-UOT is always better than MMD.

5.2 Single-Cell RNA Sequencing

We empirically evaluate the quality of our barycenter in the Single-cell RNA sequencing experiment. Single-cell RNA sequencing technique (scRNA-seq) helps us understand how the expression profile of the cells changes [58]. Barycenter estimation in the OT framework offers a principled approach to estimate the trajectory of a measure at an intermediate timestep t ($t_i < t < t_j$) when we have measurements available only at t_i (source) and t_j (target) time steps.

Dataset and experimental setup. We perform experiments on the Embryoid Body (EB) single-cell dataset [43]. The dataset has samples available at five timesteps (t_j with $j = 0, \dots, 4$), which were collected during a 25-day period of development of the human embryo. Following [68], we project the data onto two-dimensional space and associate uniform measures to the source and the target samples given at different timesteps. We consider the samples at timestep t_i and t_{i+2} as the samples from the source and target measures where $0 \leq i \leq 2$ and aim at estimating the measure at t_i timestep as their barycenter with equal interpolation weights $\rho_1 = \rho_2 = 0.5$.

We compute the barycenters using MMD-UOT (10) and the ϵ KL-UOT [13, 40] approaches. For both, a simplex constraint is used to cater to the case of uniform measures. We also compare against the empirical average of the source and target measures which is the barycenter obtained with the MMD metric.

The computed barycenter is evaluated against the measure corresponding to the ground truth samples available at the corresponding timestep. We compute the distance between the two using the MMD metric with RBF kernel [30]. The hyperparameters are chosen based on the leave-one-out validation protocol. More details are in Appendix C.3.

Results. Table 3 shows that MMD-UOT achieves the lowest distance from the ground truth for all the timesteps, illustrating its superior interpolation quality.

5.3 Domain Adaptation in JUMBOT framework

OT has been widely employed in domain adaptation problems [17, 16, 59, 21]. JUMBOT [23] is a popular domain adaptation method based on ϵ KL-UOT that outperforms OT-based baselines. JUMBOT’s loss function involves a cross-entropy term and ϵ KL-UOT discrepancy term between the source and target distributions. We showcase the utility of MMD-UOT (9) in the JUMBOT [23] framework.

Table 3: MMD distance (lower is better) between computed barycenter and the ground truth distribution. We observe that MMD-UOT’s results are closer to the ground truth than the baselines’ results at all timesteps.

Timestep	MMD	ϵ KL-UOT	MMD-UOT
t_1	0.375	0.391	0.334
t_2	0.190	0.184	0.179
t_3	0.125	0.138	0.116
Avg.	0.230	0.238	0.210

Table 4: Target domain accuracy (higher is better) obtained in domain adaptation experiments. Results for ϵ KL-UOT are reproduced from the code open-sourced for JUMBOT in [23]. MMD-UOT outperforms ϵ KL-UOT in all the domain adaptation tasks considered.

Source	Target	ϵ KL-UOT	MMD-UOT
M-MNIST	USPS	91.53	94.97
M-MNIST	MNIST	99.35	99.50
MNIST	M-MNIST	96.51	96.96
MNIST	USPS	96.51	97.01
SVHN	M-MNIST	94.26	95.35
SVHN	MNIST	98.68	98.98
SVHN	USPS	92.78	93.22
USPS	MNIST	96.76	98.53
Avg.		95.80	96.82

Dataset and experimental setup We perform the domain adaptation experiment with and Digits datasets comprising of MNIST [36], M-MNIST [26], SVHN [50], USPS [34] datasets. We replace the ϵ KL-UOT based loss with the MMD-UOT loss (9), keeping the other experimental set-up the same as JUMBOT. We obtain JUMBOT’s result with ϵ KL-UOT with the best-reported hyperparameters [23]. Following JUMBOT, we tune hyperparameters of MMD-UOT for the Digits experiment on USPS to MNIST (U→M) domain adaptation task and use the same hyperparameters for the rest of the domain adaptation tasks on Digits. More details are in Appendix C.4.

Results Table 4 reports the accuracy obtained on target datasets. We observe that MMD-UOT-based loss performs better than ϵ KL-UOT-based loss for all the domain adaptation tasks. In Appendix Figure 8, we also compare the t-SNE plot of the embeddings learnt with the MMD-UOT and ϵ KL-UOT-based loss. The clusters formed with the MMD-UOT seem better separated (for example, the red and the cyan-colored clusters).

5.4 Prompt Learning

The task of learning prompts (e.g. “a tall bird of [class]”) for vision-language models has emerged as a promising approach to adapt large pre-trained models like CLIP [57] for downstream tasks. The similarity between prompt features (which are class-specific) and visual features of a given image can help us classify the image. A recent OT-based prompt learning approach, PLOT [11], obtained state-of-the-art results on the K -shot recognition task in which only K images per class are available during training. We evaluate the performance of MMD-UOT following the setup of [11] on the benchmark EuroSAT [33] dataset consisting of satellite images, Describable Textures Dataset (DTD) having images of textures and Oxford-Pets dataset having images of pets.

Results With the same evaluation protocol as in [11], we report the classification accuracy averaged over three seeds in Table 5. We note that MMD-UOT-based prompt-learning achieves better results than PLOT, especially when K is less (more challenging case due to lesser training data). With the EuroSAT dataset, the improvement is as high as 4% for a challenging case of $K=1$. More details are in Appendix C.5.

6 Conclusion

The literature on unbalanced optimal transport (UOT) has largely focused on ϕ -divergence-based regularization. Our theoretical and empirical findings demonstrate the potential of MMD-regularization in UOT as an effective alternative

Table 5: Average and standard deviation (over 3 runs) of accuracy (higher is better) on the k -shot classification task, shown for different values of shots (k) in the state-of-the-art PLOT framework for EuroSAT, DTD and Oxford-Pets dataset. The proposed method replaces OT with MMD-UOT in PLOT, keeping all other hyperparameters the same. The results of PLOT are taken from their paper [11].

Dataset	Method	1	2	4	8	16
EuroSAT	PLOT	54.05 \pm 5.95	64.21 \pm 1.90	72.36 \pm 2.29	78.15 \pm 2.65	82.23 \pm 0.91
	Proposed	58.47 \pm 1.37	66.0 \pm 0.93	71.97 \pm 2.21	79.03 \pm 1.91	83.23 \pm 0.24
DTD	PLOT	46.55 \pm 2.62	51.24 \pm 1.95	56.03 \pm 0.43	61.70 \pm 0.35	65.60 \pm 0.82
	Proposed	47.27 \pm 1.46	51.0 \pm 1.71	56.40 \pm 0.73	63.17 \pm 0.69	65.90 \pm 0.29
Oxford-Pets	PLOT	87.49 \pm 0.57	86.64 \pm 0.63	88.63 \pm 0.26	87.39 \pm 0.74	87.21 \pm 0.40
	Proposed	87.60 \pm 0.65	87.47 \pm 1.04	88.77 \pm 0.46	87.23 \pm 0.34	88.27 \pm 0.29

to ϕ -divergence. We also theoretically show the benefits of a general family of IPM-regularized UOT. We believe that our findings will inspire further exploration in this exciting direction.

References

- [1] Agrawal, R., Horel, T.: Optimal bounds between f-divergences and integral probability metrics. In: ICML 2020 (2020)
- [2] Agueh, M., Carlier, G.: Barycenters in the wasserstein space. *SIAM Journal on Mathematical Analysis* **43**(2), 904–924 (2011)
- [3] Arase, Y., Bao, H., Yokoi, S.: Unbalanced optimal transport for unbalanced word alignment. In: ACL 2023 (2023)
- [4] Balaji, Y., Chellappa, R., Feizi, S.: Robust optimal transport with applications in generative modeling and domain adaptation. In: NeurIPS 2020 (2020)
- [5] Beck, A., Teboulle, M.: A fast iterative shrinkage-thresholding algorithm for linear inverse problems. *SIAM Journal on Imaging Sciences* **2**(1), 183–202 (2009)
- [6] Ben-Tal, A., Nemirovski, A.: *Lectures On Modern Convex Optimization* (2021)
- [7] Bian, Y., Wang, J., Jun, J.J., Xie, X.Q.: Deep convolutional generative adversarial network (dcgan) models for screening and design of small molecules targeting cannabinoid receptors. *Molecular Pharmaceutics* **16**(11), 4451–4460 (2019)
- [8] Bietti, A., Mairal, J.: Group invariance, stability to deformations, and complexity of deep convolutional representations. *Journal of Machine Learning Research* **20**, 25:1–25:49 (2017)
- [9] Bietti, A., Mialon, G., Chen, D., Mairal, J.: A kernel perspective for regularizing deep neural networks. In: ICML 2019 (2019)
- [10] Bottou, L., Arjovsky, M., Lopez-Paz, D., Oquab, M.: Geometrical insights for implicit generative modeling. *Braverman Readings in Machine Learning 2017* pp. 229–268 (2017)
- [11] Chen, G., Yao, W., Song, X., Li, X., Rao, Y., Zhang, K.: Prompt learning with optimal transport for vision-language models. In: ICLR 2023 (2023)
- [12] Chen, Y., Lan, Y., Xiong, R., Pang, L., Ma, Z., Cheng, X.: Evaluating natural language generation via unbalanced optimal transport. In: IJCAI 2020 (2020)
- [13] Chizat, L., Peyre, G., Schmitzer, B., Vialard, F.X.: Unbalanced optimal transport: Dynamic and kantovich formulations. *Journal of Functional Analysis* **274**(11), 3090–3123 (2018)
- [14] Chizat, L.: Unbalanced optimal transport : Models, numerical methods, applications. Tech. rep., Universite Paris sciences et lettres (2017)
- [15] Chizat, L., Peyré, G., Schmitzer, B., Vialard, F.X.: Scaling algorithms for unbalanced optimal transport problems. *Math. Comput.* **87**(314), 2563–2609 (2018)
- [16] Courty, N., Flamary, R., Tuia, D., Rakotomamonjy, A.: Optimal transport for domain adaptation. *IEEE Transactions on Pattern Analysis and Machine Intelligence* **39**(9), 1853–1865 (2017)

- [17] Courty, N., Flamary, R., Habrard, A., Rakotomamonjy, A.: Joint distribution optimal transportation for domain adaptation. In: NIPS 2017 (2017)
- [18] Csiszar, I.: Information-type measures of difference of probability distributions and indirect observations. *Studia Scientiarum Mathematicarum Hungarica* **2**, 299–318 (1967)
- [19] Cuturi, M.: Sinkhorn distances: Lightspeed computation of optimal transport. In: NIPS 2013 (2013)
- [20] Cuturi, M., Doucet, A.: Fast computation of wasserstein barycenters. In: ICML 2014 (2014)
- [21] Damodaran, B.B., Kellenberger, B., Flamary, R., Tuia, D., Courty, N.: DeepJDOT: Deep Joint Distribution Optimal Transport for Unsupervised Domain Adaptation. In: ECCV 2018 (2018)
- [22] Ernst, M.D.: Permutation Methods: A Basis for Exact Inference. *Statistical Science* **19**(4), 676 – 685 (2004)
- [23] Fatras, K., Séjourné, T., Courty, N., Flamary, R.: Unbalanced minibatch optimal transport; applications to domain adaptation. In: ICML 2021 (2021)
- [24] Flamary, R., Courty, N., Gramfort, A., Alaya, M.Z., Boissunon, A., Chambon, S., Chapel, L., Corenflos, A., Fatras, K., Fournier, N., Gautheron, L., Gayraud, N.T., Janati, H., Rakotomamonjy, A., Redko, I., Rolet, A., Schutz, A., Seguy, V., Sutherland, D.J., Tavenard, R., Tong, A., Vayer, T.: Pot: Python optimal transport. *Journal of Machine Learning Research* **22**(78), 1–8 (2021)
- [25] Frogner, C., Zhang, C., Mobahi, H., Araya-Polo, M., Poggio, T.: Learning with a wasserstein loss. In: NIPS 2015 (2015)
- [26] Ganin, Y., Ustinova, E., Ajakan, H., Germain, P., Larochelle, H., Laviolette, F., Marchand, M., Lempitsky, V.: Domain-adversarial training of neural networks. *Journal of Machine Learning Research* **17**(1), 2096–2030 (2016)
- [27] Georgiou, T.T., Karlsson, J., Takyar, M.S.: Metrics for power spectra: An axiomatic approach. *IEEE Transactions on Signal Processing* **57**(3), 859–867 (2009)
- [28] Gramfort, A., Peyré, G., Cuturi, M.: Fast optimal transport averaging of neuroimaging data. In: Proceedings of 24th International Conference on Information Processing in Medical Imaging (2015)
- [29] Gretton, A., Borgwardt, K.M., Rasch, M., Schölkopf, B., Smola, A.J.: A kernel method for the two-sample-problem. In: NIPS 2006 (2006)
- [30] Gretton, A., Borgwardt, K.M., Rasch, M.J., Schölkopf, B., Smola, A.: A kernel two-sample test. *Journal of Machine Learning Research* **13**(25), 723–773 (2012)
- [31] Gulrajani, I., Ahmed, F., Arjovsky, M., Dumoulin, V., Courville, A.C.: Improved training of wasserstein gans. In: NIPS 2017 (2017)
- [32] Hanin, L.G.: Kantorovich-rubinstein norm and its application in the theory of lipschitz spaces. In: Proceedings of the Americal Mathematical Society. vol. 115 (1992)
- [33] Helber, P., Bischke, B., Dengel, A., Borth, D.: Introducing eurosat: A novel dataset and deep learning benchmark for land use and land cover classification. In: IGARSS 2018-2018 IEEE International Geoscience and Remote Sensing Symposium. pp. 204–207. IEEE (2018)
- [34] Hull, J.: A database for handwritten text recognition research. *IEEE Transactions on Pattern Analysis and Machine Intelligence* **16**(5), 550–554 (1994)
- [35] Le, K., Nguyen, H., Nguyen, Q.M., Pham, T., Bui, H., Ho, N.: On robust optimal transport: Computational complexity and barycenter computation. In: NeurIPS 2021 (2021)
- [36] LeCun, Y., Cortes, C.: MNIST handwritten digit database. <http://yann.lecun.com/exdb/mnist/> (2010)
- [37] Li, C.L., Chang, W.C., Cheng, Y., Yang, Y., Póczos, B.: MMD GAN: Towards Deeper Understanding of Moment Matching Network. In: NIPS 2017 (2017)
- [38] Li, Y., Pogodin, R., Sutherland, D.J., Gretton, A.: Self-supervised learning with kernel dependence maximization. In: NeurIPS 2021 (2021)
- [39] Liero, M., Mielke, A., Savaré, G.: Optimal transport in competition with reaction: The hellinger-kantorovich distance and geodesic curves. *SIAM J. Math. Anal.* **48**, 2869–2911 (2016)
- [40] Liero, M., Mielke, A., Savaré, G.: Optimal entropy-transport problems and a new hellinger–kantorovich distance between positive measures. *Inventiones mathematicae* **211**(3), 969–1117 (2018)
- [41] Liu, F., Xu, W., Lu, J., Zhang, G., Gretton, A., Sutherland, D.J.: Learning deep kernels for non-parametric two-sample tests. In: ICML 2020 (2020)
- [42] Miyato, T., Kataoka, T., Koyama, M., Yoshida, Y.: Spectral normalization for generative adversarial networks. In: ICLR 2018 (2018)

- [43] Moon, K.R., van Dijk, D., Wang, Z., Gigante, S., Burkhardt, D.B., Chen, W.S., Yim, K., van den Elzen, A., Hirn, M.J., Coifman, R.R., Ivanova, N.B., Wolf, G., Krishnaswamy, S.: Visualizing structure and transitions for biological data exploration. *Nature Biotechnology* **37**(12), 1482–1492 (2019)
- [44] Mroueh, Y., Rigotti, M.: Unbalanced sobolev descent. In: *NeurIPS 2020* (2020)
- [45] Muandet, K., Fukumizu, K., Sriperumbudur, B., Schölkopf, B.: Kernel mean embedding of distributions: A review and beyond. *Foundations and Trends® in Machine Learning* **10**(1-2), 1–141 (2017)
- [46] Muller, A.: Integral probability metrics and their generating classes of functions. *Advances in Applied Probability* **29**, 429–443 (1997)
- [47] Nath, J.S., Jawanpuria, P.K.: Statistical optimal transport posed as learning kernel embedding. In: *NeurIPS 2020* (2020)
- [48] Nesterov, Y.: *Introductory lectures on convex optimization: A basic course*, vol. 87. Springer Science & Business Media (2003)
- [49] Nesterov, Y.E.: A method for solving the convex programming problem with convergence rate $O(1/k^2)$. In: *Dokl. akad. nauk Sssr*. vol. 269, pp. 543–547 (1983)
- [50] Netzer, Y., Wang, T., Coates, A., Bissacco, A., Wu, B., Ng, A.: Reading digits in natural images with unsupervised feature learning. In: *NeurIPS 2011* (2011)
- [51] Nguyen, T.T., Gupta, S., Venkatesh, S.: Distributional reinforcement learning via moment matching. In: *AAAI 2021* (2021)
- [52] Niles-Weed, J., Rigollet, P.: Estimation of Wasserstein distances in the spiked transport model. In: *Bernoulli* (2019)
- [53] Peyré, G., Cuturi, M.: Computational optimal transport. *Foundations and Trends® in Machine Learning* **11**(5-6), 355–607 (2019)
- [54] Pham, K., Le, K., Ho, N., Pham, T., Bui, H.: On unbalanced optimal transport: An analysis of sinkhorn algorithm. In: *ICML 2020* (2020)
- [55] Piccoli, B., Rossi, F.: Generalized wasserstein distance and its application to transport equations with source. *Archive for Rational Mechanics and Analysis* **211**, 335–358 (2014)
- [56] Piccoli, B., Rossi, F.: On properties of the generalized wasserstein distance. *Archive for Rational Mechanics and Analysis* **222** (12 2016)
- [57] Radford, A., Kim, J.W., Hallacy, C., Ramesh, A., Goh, G., Agarwal, S., Sastry, G., Askell, A., Mishkin, P., Clark, J., Krueger, G., Sutskever, I.: Learning transferable visual models from natural language supervision. In: *ICML 2021* (2021)
- [58] Schiebinger, G., Shu, J., Tabaka, M., Cleary, B., Subramanian, V., Solomon, A., Gould, J., Liu, S., Lin, S., Berube, P., Lee, L., Chen, J., Brumbaugh, J., Rigollet, P., Hochedlinger, K., Jaenisch, R., Regev, A., Lander, E.S.: Optimal-transport analysis of single-cell gene expression identifies developmental trajectories in reprogramming. *Cell* **176**(4), 928–943.e22 (2019)
- [59] Seguy, V., Damodaran, B.B., Flamary, R., Courty, N., Rolet, A., Blondel, M.: Large-scale optimal transport and mapping estimation. In: *ICLR 2018* (2018)
- [60] Simon-Gabriel, C.J., Barp, A., Schölkopf, B., Mackey, L.: Metrizing weak convergence with maximum mean discrepancies (2020). <https://doi.org/10.48550/ARXIV.2006.09268>
- [61] Smola, A.J., Gretton, A., Song, L., Schölkopf, B.: A hilbert space embedding for distributions. In: *ALT 2007* (2007)
- [62] Solomon, J., de Goes, F., Peyré, G., Cuturi, M., Butscher, A., Nguyen, A., Du, T., Guibas, L.: Convolutional wasserstein distances: Efficient optimal transportation on geometric domains. *ACM Trans. Graph.* **34**(4) (2015)
- [63] Solomon, J., Rustamov, R., Guibas, L., Butscher, A.: Wasserstein propagation for semi-supervised learning. In: *ICML 2014* (2014)
- [64] Song, L.: *Learning via hilbert space embedding of distributions*. In: *PhD Thesis* (2008)
- [65] Sriperumbudur, B., Fukumizu, K., Gretton, A., Schölkopf, B., Lanckriet, G.: On the empirical estimation of integral probability metrics. *Electronic Journal of Statistics* **6**, 1550–1599 (2012)
- [66] Sriperumbudur, B.K., Fukumizu, K., Gretton, A., Schölkopf, B., Lanckriet, G.R.G.: On integral probability metrics, phi-divergences and binary classification. *arXiv preprint arXiv:0901.2698* (2009)

- [67] Sriperumbudur, B.K., Fukumizu, K., Lanckriet, G.R.G.: Universality, characteristic kernels and RKHS embedding of measures. *Journal of Machine Learning Research* **12**, 2389–2410 (2011)
- [68] Tong, A., Huang, J., Wolf, G., Van Dijk, D., Krishnaswamy, S.: TrajectoryNet: A dynamic optimal transport network for modeling cellular dynamics. In: *ICML 2020* (2020)
- [69] Villani, C.: *Optimal Transport: Old and New*. A series of Comprehensive Studies in Mathematics, Springer (2009)

A Preliminaries

A.1 Integral Probability Metric (IPM):

Given a set $\mathcal{G} \subset \mathcal{L}(\mathcal{X})$, the integral probability metric (IPM) [46, 66, 1] associated with \mathcal{G} , is defined by:

$$\gamma_{\mathcal{G}}(s_0, t_0) \equiv \max_{f \in \mathcal{G}} \left| \int_{\mathcal{X}} f \, ds_0 - \int_{\mathcal{X}} f \, dt_0 \right| \quad \forall s_0, t_0 \in \mathcal{R}^+(\mathcal{X}). \quad (11)$$

\mathcal{G} is called the generating set of the IPM, $\gamma_{\mathcal{G}}$.

In order that the IPM metrizes weak convergence, we assume the following [46]:

Assumption A.1. \mathcal{G} is dense in $\mathcal{C}(\mathcal{X})$ and is compact.

Since the IPM generated by \mathcal{G} and its absolute convex hull is the same (without loss of generality), we additionally assume the following:

Assumption A.2. \mathcal{G} is absolutely convex.

Remark A.3. We note that the assumptions A.1 and A.2 are needed only to generalize our theoretical results to an IPM-regularized UOT formulation (Formulation 12). These assumptions are not needed for the MMD-regularized UOT (Formulation 6).

A.2 Classical Examples of IPMs

- **Maximum Mean Discrepancy (MMD):** Let k be a characteristic kernel [67] over the domain \mathcal{X} , let $\|f\|$ denote the norm of f in the canonical reproducing kernel Hilbert space (RKHS), \mathcal{H}_k , corresponding to k . MMD is the IPM associated with the generating set: $\mathcal{G}_k \equiv \{f \in \mathcal{H}_k \mid \|f\| \leq 1\}$.

$$\text{MMD}(s_0, t_0) \equiv \max_{f \in \mathcal{G}_k} \left| \int_{\mathcal{X}} f \, ds_0 - \int_{\mathcal{X}} f \, dt_0 \right|.$$

MMD can be computed analytically in terms of evaluations of the kernel k :

$$\text{MMD}^2(s_0, t_0) = \mathbb{E}_{X \sim s_0, X' \sim s_0} [k(X, X')] + \mathbb{E}_{Y \sim t_0, Y' \sim t_0} [k(Y, Y')] - 2\mathbb{E}_{X \sim s_0, Y \sim t_0} [k(X, Y)].$$

- **Kantorovich metric (\mathcal{K}_c):** Kantorovich metric also belongs to the family of integral probability metrics associated with the generating set $\mathcal{W}_c \equiv \left\{ f : \mathcal{X} \mapsto \mathbb{R} \mid \max_{x \in \mathcal{X} \neq y \in \mathcal{X}} \frac{|f(x) - f(y)|}{c(x, y)} \leq 1 \right\}$, where c is a metric over \mathcal{X} . The Kantorovich-Fenchel duality result shows that the 1-Wasserstein metric is the same as the Kantorovich metric when restricted to probability measures.
- **Dudley:** This is the IPM associated with the generating set: $\mathcal{D}_d \equiv \{f : \mathcal{X} \mapsto \mathbb{R} \mid \|f\|_{\infty} + \|f\|_d \leq 1\}$, where d is a ground metric over $\mathcal{X} \times \mathcal{X}$. The so-called **Flat** metric is related to the Dudley metric. Its generating set is: $\mathcal{F}_d \equiv \{f : \mathcal{X} \mapsto \mathbb{R} \mid \|f\|_{\infty} \leq 1, \|f\|_d \leq 1\}$.
- **Kolmogorov:** Let $\mathcal{X} = \mathbb{R}^n$. Then, the Kolmogorov metric is the IPM associated with the generating set: $\bar{\mathcal{K}} \equiv \{1_{(-\infty, x)} \mid x \in \mathbb{R}^n\}$.
- **Total Variation (TV):** This is the IPM associated with the generating set: $\mathcal{T} \equiv \{f : \mathcal{X} \mapsto \mathbb{R} \mid \|f\|_{\infty} \leq 1\}$, where $\|f\|_{\infty} \equiv \max_{x \in \mathcal{X}} |f(x)|$. Total Variation metric over measures $s_0, t_0 \in \mathcal{R}^+(\mathcal{X})$ is defined as: $\text{TV}(s, t) \equiv \int_{\mathcal{Y}} d|s - t|(y)$, where $|s - t|(y) \equiv \begin{cases} s(y) - t(y) & \text{if } s(y) \geq t(y) \\ t(y) - s(y) & \text{otherwise} \end{cases}$

B Proofs and Additional Theory Results

As mentioned in the main paper and Remark 4.8, most of our proofs hold even with a general IPM-regularized UOT formulation (12) under mild assumptions. We re-state such results and give a general proof that holds for IPM-regularized UOT (Formulation 12), of which MMD-regularized UOT (Formulation 6) is a special case.

The proposed **IPM-regularized UOT** formulation is presented as follows.

$$\mathcal{U}_{\mathcal{G},c,\lambda_1,\lambda_2}(s_0, t_0) \equiv \min_{\pi \in \mathcal{R}^+(\mathcal{X} \times \mathcal{X})} \int c \, d\pi + \lambda_1 \gamma_{\mathcal{G}}(\pi_1, s_0) + \lambda_2 \gamma_{\mathcal{G}}(\pi_2, t_0), \quad (12)$$

where $\gamma_{\mathcal{G}}$ is defined in equation (11).

We now present the theoretical results and proofs with IPM-regularized UOT (Formulation 12), of which MMD-regularized UOT (Formulation 6) is a special case. For writing the proofs with IPM-regularized UOT, we make some additional assumptions on the generating set A.1 and A.2. To the best of our knowledge, such a analysis for IPM-regularized UOT has not been done before.

B.1 Proof of Theorem 4.1

Theorem 4.1. (Duality) *Whenever \mathcal{G} satisfies Assumptions A.1 and A.2, c is a (continuous) ground metric over compact $\mathcal{X} \times \mathcal{X}$, and $\lambda_1 = \lambda_2 = \lambda > 0$, we have that:*

$$\mathcal{U}_{\mathcal{G},c,\lambda,\lambda}(s_0, t_0) = \max_{f \in \mathcal{G}(\lambda) \cap \mathcal{W}_c} \int_{\mathcal{X}} f \, ds_0 - \int_{\mathcal{X}} f \, dt_0. \quad (13)$$

Here, $\mathcal{G}(\lambda) \equiv \{\lambda g \mid g \in \mathcal{G}\}$ and \mathcal{W}_c is all 1-Lipschitz functions wrt. metric c .

We begin by re-writing IPMs using their definitions in (6):

$$\begin{aligned} \mathcal{U}_{\mathcal{G},c,\lambda_1,\lambda_2}(s_0, t_0) &\equiv \min_{\pi \in \mathcal{R}^+(\mathcal{X} \times \mathcal{X})} \int_{\mathcal{X} \times \mathcal{X}} c \, d\pi + \lambda_1 \left(\max_{f \in \mathcal{G}} \int_{\mathcal{X}} f \, ds_0 - \int_{\mathcal{X}} f \, d\pi_1 \right) + \lambda_2 \left(\max_{g \in \mathcal{G}} \int_{\mathcal{X}} g \, dt_0 - \int_{\mathcal{X}} g \, d\pi_2 \right) \\ &= \min_{\pi \in \mathcal{R}^+(\mathcal{X} \times \mathcal{X})} \int_{\mathcal{X} \times \mathcal{X}} c \, d\pi + \left(\max_{f \in \mathcal{G}(\lambda_1)} \int_{\mathcal{X}} f \, ds_0 - \int_{\mathcal{X}} f \, d\pi_1 \right) + \left(\max_{g \in \mathcal{G}(\lambda_2)} \int_{\mathcal{X}} g \, dt_0 - \int_{\mathcal{X}} g \, d\pi_2 \right) \\ &= \max_{f \in \mathcal{G}(\lambda_1), g \in \mathcal{G}(\lambda_2)} \int_{\mathcal{X}} f \, ds_0 + \int_{\mathcal{X}} g \, dt_0 + \min_{\pi \in \mathcal{R}^+(\mathcal{X} \times \mathcal{X})} \int_{\mathcal{X} \times \mathcal{X}} c \, d\pi - \int_{\mathcal{X}} f \, d\pi_1 - \int_{\mathcal{X}} g \, d\pi_2 \\ &= \max_{f \in \mathcal{G}(\lambda_1), g \in \mathcal{G}(\lambda_2)} \int_{\mathcal{X}} f \, ds_0 + \int_{\mathcal{X}} g \, dt_0 + \min_{\pi \in \mathcal{R}^+(\mathcal{X} \times \mathcal{X})} \int_{\mathcal{X} \times \mathcal{X}} c - \bar{f} - \bar{g} \, d\pi \\ &= \max_{f \in \mathcal{G}(\lambda_1), g \in \mathcal{G}(\lambda_2)} \int_{\mathcal{X}} f \, ds_0 + \int_{\mathcal{X}} g \, dt_0 + \begin{cases} 0 & \text{if } f(x) + g(y) \leq c(x, y) \, \forall x, y \in \mathcal{X}, \\ -\infty & \text{otherwise.} \end{cases} \\ &= \max_{f \in \mathcal{G}(\lambda_1), g \in \mathcal{G}(\lambda_2)} \int_{\mathcal{X}} f \, ds_0 + \int_{\mathcal{X}} g \, dt_0, \\ &\quad \text{s.t. } f(x) + g(y) \leq c(x, y) \, \forall x, y \in \mathcal{X}. \end{aligned} \quad (14)$$

Here, $\bar{f}(x, y) \equiv f(x)$, $\bar{g}(x, y) \equiv g(y)$. The min-max interchange in the third equation is due to Sion's minimax theorem and \mathcal{G} being convex compact.

The constraints in dual, (7), are equivalent to: $g(y) \leq \min_{x \in \mathcal{X}} c(x, y) - f(x) \, \forall y \in \mathcal{X}$. The RHS is nothing but the c -conjugate (c -transform) of f . From Proposition 6 in [53], whenever c is a metric, say $c = d$, we have:

$$\min_{x \in \mathcal{X}} d(x, y) - f(x) = \begin{cases} -f(y) & \text{if } f \in \mathcal{W}_d, \\ -\infty & \text{otherwise.} \end{cases} \quad \text{Thus the constraints are equivalent to: } g(y) \leq -f(y) \, \forall y \in \mathcal{X}, f \in \mathcal{W}_d.$$

By symmetry, we also obtain that $f(y) \leq -g(y) \, \forall y \in \mathcal{X}, g \in \mathcal{W}_d$. Now, since the dual, (7), seeks to maximize the objective with respect to g , and monotonically increases with values of g ; at optimality, we have that $g(y) = -f(y) \, \forall y \in \mathcal{X}$. Note that this equality is possible to achieve as both $g, f \in \mathcal{G}(\lambda) \cap \mathcal{W}_d$. Eliminating g , one obtains (13).

Remark B.1. *If \mathcal{G} is the unit uniform-norm ball (corresponding to TV), our result specializes to that in [56], which proves that $\mathcal{U}_{\mathcal{G},c,\lambda,\lambda}$ coincides with the so-called Flat metric (or the bounded Lipschitz distance).*

Remark B.2. *If the regularizer is the Kantorovich metric², i.e., $\mathcal{G} = \mathcal{W}_c$, and $\lambda_1 = \lambda_2 = \lambda \geq 1$, then $\mathcal{U}_{\mathcal{W}_c,c,\lambda,\lambda}$ coincides with the Kantorovich metric. In other words, the Kantorovich-regularized OT is the same as the Kantorovich metric. Thus, the IPM-regularized UOT (12) provides an OT interpretation for the Kantorovich metric, which is valid for potentially un-normalized measures in $\mathcal{R}^+(\mathcal{X})$. So our result, in this case, can be viewed as a generalization of the Kantorovich-Fenchel duality result.*

²The ground metric in $\mathcal{U}_{\mathcal{G},c,\lambda,\lambda}$ must be the same as that defining the Kantorovich regularizer.

B.2 Proof of Corollary 4.2

We first derive an equivalent re-formulation of 12, which will be used in our proof.

Lemma B1.

$$\mathcal{U}_{\mathcal{G},c,\lambda_1,\lambda_2}(s_0, t_0) \equiv \min_{s,t \in \mathcal{R}^+(\mathcal{X})} |s|W_1(s, t) + \lambda_1\gamma_{\mathcal{G}}(s, s_0) + \lambda_2\gamma_{\mathcal{G}}(t, t_0), \quad (15)$$

where $W_1(s, t) \equiv \begin{cases} \bar{W}_1(\frac{s}{|s|}, \frac{t}{|t|}) & \text{if } |s| = |t|, \\ \infty & \text{otherwise.} \end{cases}$, with \bar{W}_1 as the 1-Wasserstein metric.

Proof.

$$\begin{aligned} & \min_{s,t \in \mathcal{R}^+(\mathcal{X})} |s|W_1(s, t) + \lambda_1\gamma_{\mathcal{G}}(s, s_0) + \lambda_2\gamma_{\mathcal{G}}(t, t_0) \\ &= \min_{s,t \in \mathcal{R}^+(\mathcal{X}); |s|=|t|} |s| \min_{\bar{\pi} \in \mathcal{R}_1^+(\mathcal{X} \times \mathcal{X})} \int c \, d\bar{\pi} + \lambda_1\gamma_{\mathcal{G}}(s, s_0) + \lambda_2\gamma_{\mathcal{G}}(t, t_0) \quad \text{s.t. } \bar{\pi}_1 = \frac{s}{|s|}, \bar{\pi}_2 = \frac{t}{|t|} \\ &= \min_{\eta > 0} \eta \min_{\bar{\pi} \in \mathcal{R}_1^+(\mathcal{X} \times \mathcal{X})} \int c \, d\bar{\pi} + \lambda_1\gamma_{\mathcal{G}}(\eta\bar{\pi}_1, s_0) + \lambda_2\gamma_{\mathcal{G}}(\eta\bar{\pi}_2, t_0) \\ &= \min_{\eta > 0} \min_{\bar{\pi} \in \mathcal{R}_1^+(\mathcal{X} \times \mathcal{X})} \int c \, \eta d\bar{\pi} + \lambda_1\gamma_{\mathcal{G}}(\eta\bar{\pi}_1, s_0) + \lambda_2\gamma_{\mathcal{G}}(\eta\bar{\pi}_2, t_0) \\ &= \min_{\pi \in \mathcal{R}^+(\mathcal{X} \times \mathcal{X})} \int c \, d\pi + \lambda_1\gamma_{\mathcal{G}}(\pi_1, s_0) + \lambda_2\gamma_{\mathcal{G}}(\pi_2, t_0) \end{aligned}$$

The first equality holds from the definition of W_1 : $W_1(s, t) \equiv \begin{cases} \bar{W}_1(\frac{s}{|s|}, \frac{t}{|t|}) & \text{if } |s| = |t|, \\ \infty & \text{otherwise.} \end{cases}$. Eliminating normalized versions s and t using the equality constraints and introducing η to denote their common mass gives the second equality. The last equality comes after changing the variable of optimization to $\pi \in \mathcal{R}^+(\mathcal{X} \times \mathcal{X}) \equiv \eta\bar{\pi}$. Recall that $\mathcal{R}^+(\mathcal{X})$ denotes the set of all non-negative Radon measures defined over \mathcal{X} ; while the set of all probability measures is denoted by $\mathcal{R}_1^+(\mathcal{X})$. \square

Corollary 4.2 in the main paper is restated below with the IPM-regularized UOT formulation (12), followed by its proof.

Corollary 4.2. (Metricity) *Whenever c is a (continuous) ground metric, $\mathcal{U}_{\mathcal{G},c,\lambda,\lambda}$ belongs to the family of integral probability metrics (IPMs), where the generating set is the intersection of the generating set of Kantorovich, and the scaled version of the generating set of the IPM used for regularization. Further, $\mathcal{U}_{\mathcal{G},c,\lambda,\lambda}$ is a valid norm-induced metric over measures whenever the IPM used for regularization is a norm-induced metric.*

Proof. From the duality result presented in Theorem 4.1 and the definition of IPMs 11, we have that $\mathcal{U}_{\mathcal{G},c,\lambda,\lambda}$ belongs to the family of IPMs. As IPMs are induced by semi-norms over measures [46], the only condition left to be proved is positive definiteness with $\mathcal{U}_{\mathcal{G},c,\lambda_1,\lambda_2}(s_0, t_0)$, which comes from Lemma B1. Following Lemma B1, we have that for optimal s^*, t^* in (15), $\mathcal{U}_{\mathcal{G},c,\lambda,\lambda}(s_0, t_0) = 0 \iff (i) W_1(s^*, t^*) = 0, (ii) \gamma_{\mathcal{G}}(s^*, s_0) = 0, (iii) \gamma_{\mathcal{G}}(t^*, t_0) = 0$ as each term in the RHS is non-negative. When the IPM used for regularization is a norm-induced metric (e.g. the MMD metric or the Dudley metric), the conditions (i), (ii), (iii) $\iff s^* = t^* = s_0 = t_0$. Hence, we proved that $\mathcal{U}_{\mathcal{G},c,\lambda,\lambda}$ is a norm-induced metric over measures whenever the IPM used for regularization is a norm-induced metric. \square

Remark B.3. *Recall that MMD is a valid norm-induced IPM metric whenever the kernel employed is characteristic. Hence, our proof given above shows the metricity of the MMD-regularized UOT (Formulation 6).*

B.3 Proof of Corollary 4.3

Proof. As discussed in Theorem 4.1 and Corollary 4.2, the MMD-regularized UOT (Formulation 6) is an IPM with the generating set as an intersection of the generating sets of the MMD and the Kantorovich-Wasserstein metrics. We now present special cases when MMD-regularized UOT (Formulation 6) recovers back the Kantorovich-Wasserstein metric and the MMD metric.

Recovering Kantorovich. Recall that $\mathcal{G}_k(\lambda) = \{\lambda g \mid g \in \mathcal{H}_k\}$. From the definition of $\mathcal{G}_k(\lambda)$, $f \in \mathcal{G}_k(\lambda) \implies f \in$

\mathcal{H}_k , $\|f\| \leq \lambda$. Hence, as $\lambda \rightarrow \infty$, $\mathcal{G}_k(\lambda) = \mathcal{H}_k$. Using this in the duality result of Theorem 4.1, we have the following.

$$\begin{aligned} \lim_{\lambda \rightarrow \infty} \mathcal{U}_{k,c,\lambda}(s_0, t_0) &= \lim_{\lambda \rightarrow \infty} \max_{f \in \mathcal{G}_k(\lambda) \cap \mathcal{W}_c} \int f ds_0 - \int f dt_0 = \max_{f \in \mathcal{H}_k \cap \mathcal{W}_c} \int f ds_0 - \int f dt_0 \\ &\stackrel{(1)}{=} \max_{f \in \mathcal{C}(\mathcal{X}) \cap \mathcal{W}_c} \int f ds_0 - \int f dt_0 \\ &\stackrel{(2)}{=} \max_{f \in \mathcal{W}_c} \int f ds_0 - \int f dt_0 \end{aligned}$$

Equality (1) holds because \mathcal{H}_k is dense in the set of continuous functions, $\mathcal{C}(\mathcal{X})$. For equality (2), we use that \mathcal{W}_c consists of only 1-Lipschitz continuous functions. Thus, $\forall s_0, t_0 \in \mathcal{R}^+(\mathcal{X})$, $\lim_{\lambda \rightarrow \infty} \mathcal{U}_{k,c,\lambda}(s_0, t_0) = \mathcal{K}_c(s_0, t_0)$.

Recovering MMD. We next show that when $0 < \lambda_1 = \lambda_2 = \lambda \leq 1$ and the cost metric c is such that $c(x, y) \geq \sqrt{k(x, x) + k(y, y) - 2k(x, y)} = \|\phi(x) - \phi(y)\|_{\mathcal{H}_k} \forall x, y$ (Dominating cost assumption discussed in B.4), then $\forall s_0, t_0 \in \mathcal{R}^+(\mathcal{X})$, $\mathcal{U}_{k,c,\lambda}(s_0, t_0) = \text{MMD}(s_0, t_0)$.

Let $f \in \mathcal{G}_k(\lambda) \implies f = \lambda g$ where $g \in \mathcal{H}_k$, $\|g\|_{\mathcal{H}_k} \leq 1$. This also implies that $\lambda g \in \mathcal{H}_k$ as $\lambda \in (0, 1]$.

$$\begin{aligned} |f(x) - f(y)| &= |\langle \lambda g, \phi(x) - \phi(y) \rangle| \text{ (RKHS property)} \\ &\leq |\langle g, \phi(x) - \phi(y) \rangle| \text{ (} \cdot \text{ } 0 < \lambda \leq 1 \text{)} \\ &\leq \|g\|_{\mathcal{H}_k} \|\phi(x) - \phi(y)\|_{\mathcal{H}_k^*} \text{ (Holder's Inequality)} \\ &\leq \|\phi(x) - \phi(y)\|_{\mathcal{H}_k^*} \text{ (} \cdot \text{ } \|g\|_{\mathcal{H}_k} \leq 1 \text{)} \\ &\leq c(x, y) \text{ (Dominating Cost assumption and self-duality of RKHS)} \\ &\implies f \in \mathcal{W}_c \\ &\implies \mathcal{G}_k(\lambda) \subseteq \mathcal{W}_c \\ &\implies \mathcal{G}_k(\lambda) \cap \mathcal{W}_c = \mathcal{G}_k(\lambda). \end{aligned}$$

This relation, together with the duality result shown in Theorem 4.1, implies that $\mathcal{U}_{k,c,\lambda}(s_0, t_0) = \lambda \text{MMD}(s_0, t_0)$. In B.4, we show that the Euclidean distance satisfies the dominating cost assumption when the kernel employed is the Gaussian kernel and the inputs lie on a unit-norm ball. \square

B.4 Dominating Cost Assumption with Euclidean cost and Gaussian Kernel

We present a sufficient condition for the Dominating cost assumption (used in Corollary 4.3) to be satisfied while using a Euclidean cost and a Gaussian kernel based MMD. We consider the characteristic RBF kernel, $k(x, y) = \exp(-s\|x - y\|^2)$, and show that for the hyper-parameter, $0 < s \leq 0.5$, the Euclidean cost is greater than the Kernel cost when the inputs are normalized, i.e., $\|x\| = \|y\| = 1$.

$$\begin{aligned} \|x - y\|^2 &\geq k(x, x) + k(y, y) - 2k(x, y) \\ \iff \|x\|^2 + \|y\|^2 - 2\langle x, y \rangle &\geq 2 - 2k(x, y) \\ \iff \langle x, y \rangle &\leq \exp(-2s(1 - \langle x, y \rangle)) \text{ (Assuming normalized inputs)} \end{aligned} \tag{16}$$

From Cauchy Schwarz inequality, $-\|x\|\|y\| \leq \langle x, y \rangle \leq \|x\|\|y\|$. With the assumption of normalized inputs, we have that $-1 \leq \langle x, y \rangle \leq 1$. We consider two cases based on this.

Case 1: $\langle x, y \rangle \in [-1, 0]$ In this case, condition (16) is satisfied $\forall s \geq 0$ because $k(x, y) \geq 0 \forall x, y$ with a Gaussian kernel.

Case 2: $\langle x, y \rangle \in (0, 1]$ In this case, our problem in condition (16) is to find $s \geq 0$ such that $\ln \langle x, y \rangle \leq -2s(1 - \langle x, y \rangle)$. We further consider two sub-cases and derive the required condition as follows:

Case 2A: $\langle x, y \rangle \in (0, \frac{1}{e}]$ We re-parameterize $\langle x, y \rangle = e^{-n}$ for $n \geq 1$. With this, we need to find $s \geq 0$ such that $-n \leq -2s(1 - e^{-n}) \iff n \geq 2s(1 - e^{-n})$. This is satisfied when $0 < s \leq 0.5$ because $e^{-n} \geq 1 - n$.

Case 2B: $\langle x, y \rangle \in (\frac{1}{e}, \infty)$ We re-parameterize $\langle x, y \rangle = e^{-\frac{1}{n}}$ for $n > 1$. With this, we need to find $s \geq 0$ such that $\frac{1}{n(1 - e^{-\frac{1}{n}})} \geq 2s$. We consider the function $f(n) = n(1 - e^{-\frac{1}{n}})$ for $n \geq 1$. We now show that f is an increasing function by showing that the gradient $\frac{df}{dn} = 1 - (1 + \frac{1}{n})e^{-\frac{1}{n}}$ is always non-negative.

$$\begin{aligned}
& \frac{df}{dn} \geq 0 \\
& \iff e^{\frac{1}{n}} \geq \left(1 + \frac{1}{n}\right) \\
& \iff \frac{1}{n} - \ln\left(1 + \frac{1}{n}\right) \geq 0 \\
& \iff \frac{1}{n} - (\ln(n+1) - \ln(n)) \geq 0
\end{aligned}$$

Applying the Mean Value Theorem on $g(n) = \ln n$, we get

$$\begin{aligned}
& \ln(n+1) - \ln n = (n+1-n) \frac{1}{z}, \text{ where } n \leq z \leq n+1 \\
& \implies \ln\left(1 + \frac{1}{n}\right) = \frac{1}{z} \leq \frac{1}{n} \\
& \implies \frac{df}{dn} = \frac{1}{n} - \ln\left(1 + \frac{1}{n}\right) \geq 0
\end{aligned}$$

The above shows that f is an increasing function of n . We note that $\lim_{n \rightarrow \infty} f(n) = 1$, hence, $\frac{1}{f(n)} = \frac{1}{n(1-e^{-\frac{1}{n}})} \geq 1$ which implies that condition (16) is satisfied by taking $0 < s \leq 0.5$.

B.5 Proof of Corollary 4.4

Corollary 4.4 in the main paper is restated below with the IPM-regularized UOT formulation (12), followed by its proof.

Corollary 4.4. $\mathcal{U}_{\mathcal{G},c,\lambda,\lambda}(s,t) \leq \min(\lambda\gamma_{\mathcal{G}}(s,t), \mathcal{K}_c(s,t))$.

Proof. Theorem 4.1 shows that $\mathcal{U}_{\mathcal{G},c,\lambda,\lambda}$ is an IPM whose generating set is the intersection of the generating sets of Kantorovich and the scaled version of the IPM used for regularization. Thus, from the definition of max, we have that $\mathcal{U}_{\mathcal{G},c,\lambda,\lambda}(s,t) \leq \lambda\gamma_{\mathcal{G}}(s,t)$ and $\mathcal{U}_{\mathcal{G},c,\lambda,\lambda}(s,t) \leq \mathcal{K}_c(s,t)$. This implies that $\mathcal{U}_{\mathcal{G},c,\lambda,\lambda}(s,t) \leq \min(\lambda\gamma_{\mathcal{G}}(s,t), \mathcal{K}_c(s,t))$. As a special case, $\mathcal{U}_{k,c,\lambda,\lambda}(s,t) \leq \min(\lambda\text{MMD}(s,t), \mathcal{K}_c(s,t))$. \square

B.6 Proof of Corollary 4.5

Corollary 4.5 in the main paper is restated below with the IPM-regularized UOT formulation (12), followed by its proof.

Corollary 4.5. (Weak Metrization) $\mathcal{U}_{\mathcal{G},c,\lambda,\lambda}$ metric metrizes the weak convergence of normalized measures.

Proof. For convenience of notation, we denote $\mathcal{U}_{\mathcal{G},c,\lambda,\lambda}$ by \mathcal{U} . From Corollary 4.4 in the main paper,

$$0 \leq \mathcal{U}(\beta_n, \beta) \leq \mathcal{K}_c(\beta_n, \beta)$$

From Sandwich theorem, $\lim_{\beta_n \rightarrow \beta} \mathcal{U}(\beta_n, \beta) \rightarrow 0$ as $\lim_{\beta_n \rightarrow \beta} \mathcal{K}_c(\beta_n, \beta) \rightarrow 0$ by Theorem 6.9 in [69]. \square

B.7 Proof of Corollary 4.6

Corollary 4.6 in the main paper is restated below with the IPM-regularized UOT formulation (12), followed by its proof.

Corollary 4.6. (Sample Complexity) Let us denote $\mathcal{U}_{\mathcal{G},c,\lambda,\lambda}$, defined in (6), by $\bar{\mathcal{U}}$. Let \hat{s}_m, \hat{t}_m denote the empirical estimates of $s_0, t_0 \in \mathcal{R}^+(\mathcal{X})$ respectively with m samples. Then, $\bar{\mathcal{U}}(\hat{s}_m, \hat{t}_m) \rightarrow \bar{\mathcal{U}}(s_0, t_0)$ at a rate (apart from constants) same as that of $\gamma_{\mathcal{G}}(\hat{s}_m, s_0) \rightarrow 0$.

Proof. We use metricity of $\bar{\mathcal{U}}$ proved in Corollary 4.2. From triangle inequality of the metric $\bar{\mathcal{U}}$ and Corollary 4.4 in the main paper, we have that

$$0 \leq |\bar{\mathcal{U}}(\hat{s}_m, \hat{t}_m) - \bar{\mathcal{U}}(s_0, t_0)| \leq \bar{\mathcal{U}}(\hat{s}_m, s_0) + \bar{\mathcal{U}}(t_0, \hat{t}_m) \leq \lambda(\gamma_{\mathcal{G}}(\hat{s}_m, s_0) + \gamma_{\mathcal{G}}(\hat{t}_m, t_0)).$$

Hence, by Sandwich theorem, $\bar{\mathcal{U}}(\hat{s}_m, \hat{t}_m) \rightarrow \bar{\mathcal{U}}(s_0, t_0)$ at a rate at which $\gamma_{\mathcal{G}}(\hat{s}_m, s_0) \rightarrow 0$ and $\gamma_{\mathcal{G}}(\hat{t}_m, t_0) \rightarrow 0$. If the IPM used for regularization is MMD with a normalized kernel, then $\text{MMD}(s_0, \hat{s}_m) \leq \sqrt{\frac{1}{m}} + \sqrt{\frac{2 \log(1/\delta)}{m}}$ with probability at least $1 - \delta$ [61].

From the union bound, with probability at least $1 - \delta$, $|\bar{\mathcal{U}}(s_m, t_m) - \bar{\mathcal{U}}(s_0, t_0)| \leq 2\lambda \left(\sqrt{\frac{1}{m}} + \sqrt{\frac{2 \log(2/\delta)}{m}} \right)$. \square

B.8 Proof of Lemma 4.7

Lemma 4.7 in the main paper is restated below with the IPM-regularized UOT formulation (12), followed by its proof.

Lemma 4.7. (Robustness) *Let $s_0, t_0 \in \mathcal{R}_1^+(\mathcal{X})$. Consider $s_c = \rho s_0 + (1 - \rho)\delta_z$ ($\rho \in [0, 1]$), a distribution perturbed by a Dirac outlier located at some z outside of the support of t_0 . Let $m(z) = \int c(z, y) dt_0(y)$. We have that, $\mathcal{U}_{\mathcal{G}, c, \lambda_1, \lambda_2}(s_c, t_0) \leq \rho \mathcal{U}_{\mathcal{G}, c, \lambda_1, \lambda_2}(s_0, t_0) + (1 - \rho)m(z)$.*

Proof. Let π be the solution of $\mathcal{U}_{\mathcal{G}, c, \lambda_1, \lambda_2}(s_0, t_0)$. Consider $\tilde{\pi} = \rho\pi + (1 - \rho)\delta_z \otimes t_0$. It is easy to see that $\tilde{\pi}_1 = \rho\pi_1 + (1 - \rho)\delta_z$ and $\tilde{\pi}_2 = \rho\pi_2 + (1 - \rho)t_0$.

$$\begin{aligned} \mathcal{U}_{\mathcal{G}, c, \lambda_1, \lambda_2}(s_c, t_0) &\leq \int c(x, y) d\tilde{\pi}(x, y) + \lambda_1 \gamma_{\mathcal{G}}(\tilde{\pi}_1, s_c) + \lambda_2 \gamma_{\mathcal{G}}(\tilde{\pi}_2, t_0) \text{ (Using the definition of min)} \\ &\leq \int c(x, y) d\tilde{\pi}(x, y) + \lambda_1 (\rho \gamma_{\mathcal{G}}(\pi_1, s_0) + (1 - \rho) \gamma_{\mathcal{G}}(\delta_z, \delta_z)) + \lambda_2 (\rho \gamma_{\mathcal{G}}(\pi_2, t_0) + (1 - \rho) \gamma_{\mathcal{G}}(t_0, t_0)) \\ &\quad (\because \text{IPMs are jointly convex}) \\ &= \int c(x, y) d\tilde{\pi}(x, y) + \rho (\lambda_1 \gamma_{\mathcal{G}}(\pi_1, s_0) + \lambda_2 \gamma_{\mathcal{G}}(\pi_2, t_0)) \\ &= \rho \int c(x, y) d\pi(x, y) + \int (1 - \rho) c(z, y) d(\delta_z \otimes t_0)(z, y) + \rho (\lambda_1 \gamma_{\mathcal{G}}(\pi_1, s_0) + \lambda_2 \gamma_{\mathcal{G}}(\pi_2, t_0)) \\ &= \rho \int c(x, y) d\pi(x, y) + \int (1 - \rho) c(z, y) dt_0(y) + \rho (\lambda_1 \gamma_{\mathcal{G}}(\pi_1, s_0) + \lambda_2 \gamma_{\mathcal{G}}(\pi_2, t_0)) \\ &= \rho \mathcal{U}_{\mathcal{G}, c, \lambda_1, \lambda_2}(s_0, t_0) + (1 - \rho)m(z). \end{aligned}$$

We note that $m(z)$ is finite as $t_0 \in \mathcal{R}_1^+(\mathcal{X})$. \square

B.9 More on Robustness

In Lemma 4.7, we showed the robustness property of MMD-UOT with the same assumptions on the noise model used in [23, Lemma 1] for KL-regularized UOT. We now present robustness guarantees with a different noise model.

Corollary B2. *We say a measure $q \in \mathcal{R}^+(\mathcal{X})$ is corrupted with $\rho \in [0, 1]$ fraction of noise when $q = (1 - \rho)q_c + \rho q_n$, where q_c is the clean measure and q_n is the noisy measure.*

Let $s_0, t_0 \in \mathcal{R}^+(\mathcal{X})$ be corrupted with ρ fraction of noise such that $|s_c - s_n|_{TV} \leq \epsilon_1$ and $|t_c - t_n|_{TV} \leq \epsilon_2$. We have that $\mathcal{U}_{\mathcal{G}, c, \lambda, \lambda}(s_0, t_0) \leq \mathcal{U}_{\mathcal{G}, c, \lambda, \lambda}(s_c, t_c) + \rho\beta(\epsilon_1 + \epsilon_2)$, where $\beta = \max_{f \in \mathcal{G}(\lambda) \cap \mathcal{W}_c} \|f\|_{\infty}$.

Proof. We use our duality result of $\mathcal{U}_{\mathcal{G}, c, \lambda, \lambda}$, from Theorem 4.1. We first upper-bound $\mathcal{U}_{\mathcal{G}, c, \lambda, \lambda}(s_n, t_n)$ which is later used in the proof.

$$\begin{aligned} \mathcal{U}_{\mathcal{G}, c, \lambda, \lambda}(s_n, t_n) &= \max_{f \in \mathcal{G}(\lambda) \cap \mathcal{W}_c} \int f ds_n - \int f dt_n \\ &= \max_{f \in \mathcal{G}(\lambda) \cap \mathcal{W}_c} \int f d(s_n - s_c) + \int f ds_c - \int f d(t_n - t_c) - \int f dt_c \\ &\leq \max_{f \in \mathcal{G}(\lambda) \cap \mathcal{W}_c} \int f d(s_n - s_c) + \max_{f \in \mathcal{G}(\lambda) \cap \mathcal{W}_c} \int f d(t_n - t_c) + \max_{f \in \mathcal{G}(\lambda) \cap \mathcal{W}_c} \left(\int f ds_c - \int f dt_c \right) \\ &\leq \beta(|s_c - s_n|_{TV} + |t_c - t_n|_{TV}) + \mathcal{U}_{\mathcal{G}, c, \lambda, \lambda}(s_c, t_c) \\ &= \beta(\epsilon_1 + \epsilon_2) + \mathcal{U}_{\mathcal{G}, c, \lambda, \lambda}(s_c, t_c). \end{aligned} \tag{17}$$

We now show the robustness result as follows.

$$\begin{aligned}
\mathcal{U}_{\mathcal{G},c,\lambda,\lambda}(s_0, t_0) &= \max_{f \in \mathcal{G}(\lambda) \cap \mathcal{W}_c} \int f ds_0 - \int f dt_0 \\
&= \max_{f \in \mathcal{G}(\lambda) \cap \mathcal{W}_c} (1 - \rho) \int f ds_c + \rho \int f ds_n - (1 - \rho) \int f dt_c - \rho \int f dt_n \\
&= \max_{f \in \mathcal{G}(\lambda) \cap \mathcal{W}_c} (1 - \rho) \left(\int f ds_c - \int f dt_c \right) + \rho \left(\int f ds_n - \int f dt_n \right) \\
&\leq \max_{f \in \mathcal{G}(\lambda) \cap \mathcal{W}_c} (1 - \rho) \left(\int f ds_c - \int f dt_c \right) + \max_{f \in \mathcal{G}(\lambda) \cap \mathcal{W}_c} \rho \left(\int f ds_n - \int f dt_n \right) \\
&= (1 - \rho) \mathcal{U}_{\mathcal{G},c,\lambda,\lambda}(s_c, t_c) + \rho \mathcal{U}_{\mathcal{G},c,\lambda,\lambda}(s_n, t_n) \\
&\leq (1 - \rho) \mathcal{U}_{\mathcal{G},c,\lambda,\lambda}(s_c, t_c) + \rho (\mathcal{U}_{\mathcal{G},c,\lambda,\lambda}(s_c, t_c) + \beta(\epsilon_1 + \epsilon_2)) \quad (\text{Using 17}) \\
&= \mathcal{U}_{\mathcal{G},c,\lambda,\lambda}(s_c, t_c) + \rho \beta(\epsilon_1 + \epsilon_2).
\end{aligned}$$

We note that $\beta = \max_{f \in \mathcal{G}(\lambda) \cap \mathcal{W}_c} \|f\|_\infty \leq \max_{f \in \mathcal{W}_c} \|f\|_\infty < \infty$. Also, as $\beta \leq \min \left(\max_{f \in \mathcal{G}_k(\lambda)} \|f\|_\infty, \max_{f \in \mathcal{W}_c} \|f\|_\infty \right) \leq \min \left(\lambda, \max_{f \in \mathcal{W}_c} \|f\|_\infty \right)$ (for a normalized kernel).

□

B.10 Solving Problem (8) using Mirror Descent

Problem (8) is an instance of convex program and can be solved using Mirror Descent [6], presented in Algorithm 2.

Algorithm 2 Mirror Descent for solving Problem (8)

Require: Initial $\alpha_1 \geq 0$, max iterations N .
 $f(\alpha) = \text{Tr}(\alpha \mathcal{C}_{12}^\top) + \lambda_1 \left\| \alpha \mathbf{1} - \frac{\sigma_1}{m} \mathbf{1} \right\|_{G_{11}} + \lambda_2 \left\| \alpha^\top \mathbf{1} - \frac{\sigma_2}{m} \mathbf{1} \right\|_{G_{22}}.$
for $i \leftarrow 1$ to N **do**
 if $\|\nabla f(\alpha_i)\| \neq 0$ **then**
 $s_i = 1/\|\nabla f(\alpha_i)\|_\infty.$
 else
 return $\alpha_i.$
 end if
 $\alpha_{i+1} = \alpha_i \odot e^{-s_i \nabla f(\alpha_i)}.$
end for
return $\alpha_{i+1}.$

B.11 Equivalence between Problems (8) and (9)

We comment on the equivalence between Problems (8) and (9) based on the equivalence of their Ivanov forms:

Ivanov form for Problem (8) is

$$\min_{\alpha \geq 0 \in \mathbb{R}^{m_1 \times m_2}} \text{Tr}(\alpha \mathcal{C}_{12}^\top) \text{ s.t. } \left\| \alpha \mathbf{1} - \frac{\sigma_1}{m_1} \mathbf{1} \right\|_{G_{11}} \leq r_1, \left\| \alpha^\top \mathbf{1} - \frac{\sigma_2}{m_2} \mathbf{1} \right\|_{G_{22}} \leq r_2,$$

where $r_1, r_2 > 0$.

Similarly, the Ivanov form for Problem (9) is

$$\min_{\alpha \geq 0 \in \mathbb{R}^{m_1 \times m_2}} \text{Tr}(\alpha \mathcal{C}_{12}^\top) \text{ s.t. } \left\| \alpha \mathbf{1} - \frac{\sigma_1}{m_1} \mathbf{1} \right\|_{G_{11}}^2 \leq \bar{r}_1, \left\| \alpha^\top \mathbf{1} - \frac{\sigma_2}{m_2} \mathbf{1} \right\|_{G_{22}}^2 \leq \bar{r}_2,$$

where $\bar{r}_1, \bar{r}_2 > 0$.

As we can see that the Ivanov forms are the same with $\bar{r}_1 = r_1^2, \bar{r}_2 = r_2^2$, the solutions obtained for Problems (8) and (9) are the same.

B.12 Proof of Theorem 4.9: Consistency of the Proposed Estimator

Proof. From triangle inequality,

$$|\hat{\mathcal{U}}_m(\hat{s}_m, \hat{t}_m) - \bar{\mathcal{U}}(s_0, t_0)| \leq |\hat{\mathcal{U}}_m(\hat{s}_m, \hat{t}_m) - \hat{\mathcal{U}}_m(s_0, t_0)| + |\hat{\mathcal{U}}_m(s_0, t_0) - \bar{\mathcal{U}}(s_0, t_0)|, \quad (18)$$

where $\hat{\mathcal{U}}_m(s_0, t_0)$ is same as $\bar{\mathcal{U}}(s_0, t_0)$ except that it employs the restricted feasibility set, $\mathcal{F}(\hat{s}_m, \hat{t}_m)$, for the transport plan: set of all joints supported using the samples in \hat{s}_m, \hat{t}_m alone i.e.,

$\mathcal{F}(\hat{s}_m, \hat{t}_m) \equiv \left\{ \sum_{i=1}^m \sum_{j=1}^m \alpha_{ij} \delta_{(x_{1i}, x_{2j})} \mid \alpha_{ij} \geq 0 \forall i, j = 1, \dots, m \right\}$. Here, δ_z is the dirac measure at z . We begin by bounding the first term.

We denote the (common) objective in $\hat{\mathcal{U}}_m(\cdot, \cdot), \bar{\mathcal{U}}(\cdot, \cdot)$ as a function of the transport plan, π , by $h(\pi, \cdot, \cdot)$. Then,

$$\begin{aligned} \hat{\mathcal{U}}_m(\hat{s}_m, \hat{t}_m) - \hat{\mathcal{U}}_m(s_0, t_0) &= \min_{\pi \in \mathcal{F}(\hat{s}_m, \hat{t}_m)} h(\pi, \hat{s}_m, \hat{t}_m) - \min_{\pi \in \mathcal{F}(\hat{s}_m, \hat{t}_m)} h(\pi, s_0, t_0) \\ &\leq h(\pi^*, \hat{s}_m, \hat{t}_m) - h(\pi^*, s_0, t_0) \left(\text{where } \pi^* = \arg \min_{\pi \in \mathcal{F}(\hat{s}_m, \hat{t}_m)} h(\pi, s_0, t_0) \right) \\ &= \lambda_1 (\text{MMD}(\pi_1^*, \hat{s}_m) - \text{MMD}(\pi_1^*, s_0)) + \lambda_2 (\text{MMD}(\pi_2^*, \hat{t}_m) - \text{MMD}(\pi_2^*, t_0)) \\ &\leq \lambda_1 \text{MMD}(s_0, \hat{s}_m) + \lambda_2 \text{MMD}(t_0, \hat{t}_m) \quad (\because \text{MMD satisfies triangle inequality}) \end{aligned}$$

Similarly, one can show that $\hat{\mathcal{U}}_m(s_0, t_0) - \hat{\mathcal{U}}_m(\hat{s}_m, \hat{t}_m) \leq \lambda_1 \text{MMD}(s_0, \hat{s}_m) + \lambda_2 \text{MMD}(t_0, \hat{t}_m)$. Now, [61] shows that, with probability at least $1 - \delta$, $\text{MMD}(s_0, \hat{s}_m) \leq \frac{1}{\sqrt{m}} + \sqrt{\frac{2 \log(1/\delta)}{m}}$. Hence, the first term in inequality (18) is upper-bounded by $(\lambda_1 + \lambda_2) \left(\frac{1}{\sqrt{m}} + \sqrt{\frac{2 \log 2/\delta}{m}} \right)$, with probability at least $1 - \delta$.

We next look at the second term in inequality (18): $|\hat{\mathcal{U}}_m(s_0, t_0) - \bar{\mathcal{U}}(s_0, t_0)|$. Let $\bar{\pi}^m$ be the optimal transport plan in definition of $\hat{\mathcal{U}}_m(s_0, t_0)$. Let π^* be the optimal transport plan in the definition of $\bar{\mathcal{U}}(s_0, t_0)$. Consider another transport plan: $\hat{\pi}^m \in \mathcal{F}(\hat{s}_m, \hat{t}_m)$ such that $\hat{\pi}^m(i, j) = \frac{\eta_{ij}}{m^2}$ where $\eta_{ij} = \frac{\pi^*(X_i, Y_j)}{s_0(X_i)t_0(Y_j)}$ for $i, j \in [1, m]$.

$$\begin{aligned} |\hat{\mathcal{U}}_m(s_0, t_0) - \bar{\mathcal{U}}(s_0, t_0)| &= \hat{\mathcal{U}}_m(s_0, t_0) - \bar{\mathcal{U}}(s_0, t_0) \\ &= h(\bar{\pi}^m, s_0, t_0) - h(\pi^*, s_0, t_0) \\ &\leq h(\hat{\pi}^m, s_0, t_0) - h(\pi^*, s_0, t_0) \quad (\because \bar{\pi}^m \text{ is optimal,}) \\ &\leq \langle \mu_k(\hat{\pi}^m) - \mu_k(\pi^*), c \rangle + \lambda_1 \|\mu_k(\hat{\pi}_1^m) - \mu_k(\pi_1^*)\|_{\mathcal{H}_k} + \lambda_2 \|\mu_k(\hat{\pi}_2^m) - \mu_k(\pi_2^*)\|_{\mathcal{H}_k} \\ &\leq \|\mu_k(\hat{\pi}^m) - \mu_k(\pi^*)\|_{\mathcal{H}_k} \|c\|_{\mathcal{H}_k} + \lambda_1 \|\mu_k(\hat{\pi}_1^m) - \mu_k(\pi_1^*)\|_{\mathcal{H}_k} + \lambda_2 \|\mu_k(\hat{\pi}_2^m) - \mu_k(\pi_2^*)\|_{\mathcal{H}_k} \end{aligned}$$

The second last inequality comes from the triangle inequality of MMD. For the last inequality, we apply Holder's inequality. We now upper-bound the MMD distance between $\hat{\pi}^m$ and π^* .

$$\begin{aligned} \|\mu_k(\hat{\pi}^m) - \mu_k(\pi^*)\|_{\mathcal{H}_k} &= \max_{f \in \mathcal{H}_k, \|f\|_{\mathcal{H}_k} \leq 1} \left| \int f d\hat{\pi}^m - \int f d\pi^* \right| \\ &= \max_{f \in \mathcal{H}_k, \|f\|_{\mathcal{H}_k} \leq 1} \int f d\hat{\pi}^m - \int f d\pi^* \\ &= \max_{f \in \mathcal{H}_k, \|f\|_{\mathcal{H}_k} \leq 1} \sum_{i=1}^m \sum_{j=1}^m f(X_i, Y_j) \frac{\pi^*(x_i, y_j)}{m^2 s_0(x_i) t_0(y_j)} - \int \int f(x, y) \frac{\pi^*(x, y)}{s_0(x) t_0(y)} s_0(x) t_0(y) dx dy \\ &= \max_{f \in \mathcal{H}_k, \|f\|_{\mathcal{H}_k} \leq 1} \mathbb{E}_{X \sim \hat{s}_m, Y \sim \hat{t}_m} \left[f(X, Y) \frac{\pi^*(X, Y)}{s_0(X) t_0(Y)} \right] - \mathbb{E}_{X \sim s_0, Y \sim t_0} \left[f(X, Y) \frac{\pi^*(X, Y)}{s_0(X) t_0(Y)} \right] \\ &= \max_{f \in \mathcal{H}_k, \|f\|_{\mathcal{H}_k} \leq 1} \mathbb{E}_{X \sim \hat{s}_m, Y \sim \hat{t}_m} [f(X, Y) \eta(X, Y)] - \mathbb{E}_{X \sim s_0, Y \sim t_0} [f(X, Y) \eta(X, Y)] \end{aligned}$$

As we assume η can be embedded in \mathcal{H}_k , $\|\eta\|_{\mathcal{H}_k} < \infty$.

$$\begin{aligned}
\|\mu_k(\hat{\pi}^m) - \mu_k(\pi^*)\|_{\mathcal{H}_k} &= \max_{f \in \mathcal{H}_k, \|f\|_{\mathcal{H}_k} \leq 1} \langle f \otimes \eta, \mathbb{E}_{X \sim \hat{s}_m, Y \sim \hat{t}_m} [\phi(X) \otimes \phi(Y)] - \mathbb{E}_{X \sim s_0, Y \sim t_0} [\phi(X) \otimes \phi(Y)] \rangle \\
&\leq \|f \otimes \eta\|_{\mathcal{H}_k} \|\mathbb{E}_{X \sim \hat{s}_m, Y \sim \hat{t}_m} [\phi(X) \otimes \phi(Y)] - \mathbb{E}_{X \sim s_0, Y \sim t_0} [\phi(X) \otimes \phi(Y)]\|_{\mathcal{H}_k} \quad (\text{Holder's Inequality}) \\
&\leq \|\eta\|_{\mathcal{H}_k} \|\mathbb{E}_{X \sim \hat{s}_m, Y \sim \hat{t}_m} [\phi(X) \otimes \phi(Y)] - \mathbb{E}_{X \sim s_0, Y \sim t_0} [\phi(X) \otimes \phi(Y)]\|_{\mathcal{H}_k} \\
&= \|\eta\|_{\mathcal{H}_k} \|\mu_k(\hat{s}_m) \otimes \mu_k(\hat{t}_m) - \mu_k(s_0) \otimes \mu_k(t_0)\|_{\mathcal{H}_k} \\
&= \|\eta\|_{\mathcal{H}_k} \|\mu_k(\hat{s}_m) \otimes (\mu_k(\hat{t}_m) - \mu_k(t_0)) + (\mu_k(\hat{s}_m) - \mu_k(s_0)) \otimes \mu_k(t_0)\|_{\mathcal{H}_k} \\
&\leq \|\eta\|_{\mathcal{H}_k} (\|\mu_k(\hat{s}_m)\|_{\mathcal{H}_k} \|\mu_k(\hat{t}_m) - \mu_k(t_0)\|_{\mathcal{H}_k} + \|\mu_k(t_0)\|_{\mathcal{H}_k} \|\mu_k(\hat{s}_m) - \mu_k(s_0)\|_{\mathcal{H}_k}) \\
&\quad (\text{Triangle Inequality}) \\
&\leq \|\eta\|_{\mathcal{H}_k} (\|\mu_k(\hat{t}_m) - \mu_k(t_0)\|_{\mathcal{H}_k} + \|\mu_k(\hat{s}_m) - \mu_k(s_0)\|_{\mathcal{H}_k}) \quad (\text{With a normalized kernel})
\end{aligned}$$

From the union bound, with probability at least $1 - \delta$, $\|\mu_k(\hat{\pi}^m) - \mu_k(\pi^*)\|_{\mathcal{H}_k} \leq 2\|\eta\|_{\mathcal{H}_k} \left(\sqrt{\frac{1}{m}} + \sqrt{\frac{2 \log(2/\delta)}{m}} \right)$.

Similarly, with the probability at least $1 - \delta$, $\|\mu_k(\hat{\pi}_1^m) - \mu_k(\pi_1^*)\|_{\mathcal{H}_k} \leq 2\|\eta_1\|_{\mathcal{H}_k} \left(\sqrt{\frac{1}{m}} + \sqrt{\frac{2 \log(2/\delta)}{m}} \right)$ where

$$\eta_1(x) = \frac{\pi_1^*(x)}{s_0(x)}; \text{ and with the probability at least } 1 - \delta, \|\mu_k(\hat{\pi}_2^m) - \mu_k(\pi_2^*)\|_{\mathcal{H}_k} \leq 2\|\eta_2\|_{\mathcal{H}_k} \left(\sqrt{\frac{1}{m}} + \sqrt{\frac{2 \log(2/\delta)}{m}} \right)$$

where $\eta_2(y) = \frac{\pi_2^*(y)}{t_0(y)}$.

Hence, with probability at least $1 - \delta$,

$$|\hat{\mathcal{U}}_m(s_0, t_0) - \bar{\mathcal{U}}(s_0, t_0)| \leq \frac{2}{\sqrt{m}} (\|c\|_{\mathcal{H}_k} \|\eta\|_{\mathcal{H}_k} + \lambda_1 \|\eta_1\|_{\mathcal{H}_k} + \lambda_2 \|\eta_2\|_{\mathcal{H}_k}) \left(1 + \sqrt{2 \log 6/\delta} \right).$$

Applying union bound, we get that with probability at least $1 - \delta$, the estimation error, $|\hat{\mathcal{U}}_m(\hat{s}_m, \hat{t}_m) - \bar{\mathcal{U}}(s_0, t_0)|$, is upper-bounded by $\frac{1}{\sqrt{m}} (\|c\|_{\mathcal{H}_k} \|\eta\|_{\mathcal{H}_k} + \lambda_1 \|\eta_1\|_{\mathcal{H}_k} + \lambda_2 \|\eta_2\|_{\mathcal{H}_k} + \lambda_1 + \lambda_2) \left(1 + \sqrt{2 \log 8/\delta} \right)$. This completes the proof. \square

B.13 Proof of Lemma 4.10

Proof. Let $f(\alpha)$ denote the objective of Problem (9), G_{11}, G_{22} are the Gram matrices over the source and target samples, respectively and m_1, m_2 as the number of source and target samples respectively.

$$\nabla f(\alpha) = \mathcal{C}_{12} + 2 \left(\lambda_1 G_{11} \left(\alpha \mathbf{1}_{m_2} - \frac{\sigma_1}{m_1} \mathbf{1}_{m_1} \right) \mathbf{1}_{m_2}^\top + \lambda_2 \mathbf{1}_{m_1} \left(\mathbf{1}_{m_1}^\top \alpha - \mathbf{1}_{m_2}^\top \frac{\sigma_2}{m_2} \right) G_{22} \right)$$

We now derive the Lipschitz constant of this gradient.

$$\begin{aligned}
\nabla f(\alpha) - \nabla f(\beta) &= 2 (\lambda_1 G_{11} (\alpha - \beta) \mathbf{1}_{m_2} \mathbf{1}_{m_2}^\top + \mathbf{1}_{m_1} \mathbf{1}_{m_1}^\top \lambda_2 (\alpha - \beta) G_{22}) \\
\text{vec}((\nabla f(\alpha) - \nabla f(\beta))^\top) &= 2 \left(\lambda_1 \text{vec}((G_{11} (\alpha - \beta) \mathbf{1}_{m_2} \mathbf{1}_{m_2}^\top)^\top) + \lambda_2 \text{vec}((\mathbf{1}_{m_1} \mathbf{1}_{m_1}^\top (\alpha - \beta) G_{22})^\top) \right) \\
&= 2 (\lambda_1 \mathbf{1}_{m_2} \mathbf{1}_{m_2}^\top \otimes G_{11} + \lambda_2 G_{22} \otimes \mathbf{1}_{m_1} \mathbf{1}_{m_1}^\top) \text{vec}(\alpha - \beta)
\end{aligned}$$

where \otimes denotes Kronecker product.

$$\begin{aligned}
\|\text{vec}(\nabla f(\alpha) - \nabla f(\beta))\|_F &= \|\text{vec}((\nabla f(\alpha) - \nabla f(\beta))^\top)\|_F \\
&\leq 2 \|\lambda_1 \mathbf{1}_{m_2} \mathbf{1}_{m_2}^\top \otimes G_{11} + \lambda_2 G_{22} \otimes \mathbf{1}_{m_1} \mathbf{1}_{m_1}^\top\|_F \|\text{vec}(\alpha - \beta)\|_F \quad (\text{Cauchy Schwarz}).
\end{aligned}$$

This implies the Lipschitz smoothness constant

$$\begin{aligned}
L &= 2 \|\lambda_1 \mathbf{1}_{m_2} \mathbf{1}_{m_2}^\top \otimes G_{11} + \lambda_2 G_{22} \otimes \mathbf{1}_{m_1} \mathbf{1}_{m_1}^\top\|_F \\
&= 2 \sqrt{(\lambda_1 m_2)^2 \|G_{11}\|_F^2 + (\lambda_2 m_1)^2 \|G_{22}\|_F^2 + 2 \lambda_1 \lambda_2 \langle \mathbf{1}_{m_2} \mathbf{1}_{m_2}^\top \otimes G_{11}, G_{22} \otimes \mathbf{1}_{m_1} \mathbf{1}_{m_1}^\top \rangle_F} \\
&= 2 \sqrt{(\lambda_1 m_2)^2 \|G_{11}\|_F^2 + (\lambda_2 m_1)^2 \|G_{22}\|_F^2 + 2 \lambda_1 \lambda_2 (\mathbf{1}_{m_1}^\top G_{11} \mathbf{1}_{m_1}) (\mathbf{1}_{m_2}^\top G_{22} \mathbf{1}_{m_2})}.
\end{aligned}$$

For the last equality, we use the following properties for Kronecker products-

Mixed product property: $(A \otimes B)^\top = A^\top \otimes B^\top$, $(A \otimes B)(C \otimes D) = (AC) \otimes (BD)$ and Spectrum property: $\text{Tr}((AC) \otimes (BD)) = \text{Tr}(AC) \text{Tr}(BD)$. \square

B.14 Solving Problem (9) using Accelerated Projected Gradient Descent

In Algorithm 1, we present the accelerated projected gradient descent (APGD) algorithm that we use to solve Problem (9), as discussed in Section 4.2. The projection operation involved is $\text{Project}_{\geq 0}(\mathbf{x}) = \max(\mathbf{x}, 0)$.

B.15 More on the Barycenter problem

B.15.1 Proof of Lemma 4.11

Proof. We propose estimating the barycenter with the restriction that the transport plan π^i corresponding to $\hat{\mathcal{U}}(\hat{s}_i, s)$ is supported on $\mathcal{D}_i \times \cup_{i=1}^n \mathcal{D}_i$. Following [20], we assume³ that the barycenter, s , is supported on $\cup_{i=1}^n \mathcal{D}_i$ and $\beta \in \mathbb{R}^m$ denotes the corresponding probabilities. With $\hat{\mathcal{U}}_m$ as defined in Equation (8), the MMD-UOT barycenter formulation, $\hat{\mathcal{B}}_m(\hat{s}_1, \dots, \hat{s}_n) = \min_{s \in \mathcal{R}^+(\mathcal{X})} \sum_{i=1}^n \rho_i \hat{\mathcal{U}}_m(\hat{s}_i, s)$, becomes

$$\min_{\alpha_1, \dots, \alpha_n, \beta \geq 0} \sum_{i=1}^n \rho_i \left\{ \text{Tr}(\alpha_i \mathcal{C}_i^\top) + \lambda_1 \|\alpha_i \mathbf{1} - \frac{\sigma_i}{m_i} \mathbf{1}\|_{G_{ii}}^2 + \lambda_2 \|\alpha_i^\top \mathbf{1} - \beta\|_G^2 \right\}. \quad (19)$$

Following our discussion in Sections 4.2 and B.11, we present an equivalent barycenter formulation with squared-MMD regularization. This not only makes the objective smooth allowing us to exploit accelerated solvers, but also simplifies the problem, as we discuss next.

$$\mathcal{B}'_m(\hat{s}_1, \dots, \hat{s}_n) \equiv \min_{\alpha_1, \dots, \alpha_n, \beta \geq 0} \sum_{i=1}^n \rho_i \left\{ \text{Tr}(\alpha_i \mathcal{C}_i^\top) + \lambda_1 \|\alpha_i \mathbf{1} - \frac{\sigma_i}{m_i} \mathbf{1}\|_{G_{ii}}^2 + \lambda_2 \|\alpha_i^\top \mathbf{1} - \beta\|_G^2 \right\}. \quad (20)$$

The above problem is a least squares problem in terms of β with a non-negativity constraint. Equating the gradient wrt β as 0, we get $G(\beta - \sum_{j=1}^n \rho_j \alpha_j^\top \mathbf{1}) = 0$. As the Gram matrices of universal kernels are full-rank [64, Corollary 32], this implies $\beta = \sum_{j=1}^n \rho_j \alpha_j^\top \mathbf{1}$, which also satisfies the non-negativity constraint. Substituting $\beta = \sum_{j=1}^n \rho_j \alpha_j^\top \mathbf{1}$ in 20 gives us the MMD-UOT barycenter formulation:

$$\mathcal{B}'_m(\hat{s}_1, \dots, \hat{s}_n) \equiv \min_{\alpha_1, \dots, \alpha_n, \beta \geq 0} \sum_{i=1}^n \rho_i \left\{ \text{Tr}(\alpha_i \mathcal{C}_i^\top) + \lambda_1 \|\alpha_i \mathbf{1} - \frac{\sigma_i}{m_i} \mathbf{1}\|_{G_{ii}}^2 + \lambda_2 \|\alpha_i^\top \mathbf{1} - \sum_{j=1}^n \rho_j \alpha_j^\top \mathbf{1}\|_G^2 \right\}. \quad (21)$$

□

B.15.2 Solving the Barycenter Formulation

The objective of 21, as a function of α_i , has the following smoothness constant (derivation analogous to Lemma 4.10 in the main paper).

$$L_i = 2\rho_i \sqrt{(\lambda_1 m)^2 \|G_{ii}\|_F^2 + (\eta_i m_i)^2 \|G\|_F^2 + 2\lambda_1 \eta_i (\mathbf{1}_{m_i}^\top G_{ii} \mathbf{1}_{m_i})(\mathbf{1}_m^\top G \mathbf{1}_m)}$$

where $\eta_i = \lambda_2(1 - \rho_i)$. We jointly optimize for α_i 's using accelerated projected gradient descent with step-size $1/L_i$.

B.15.3 Consistency of the sample-based estimator

Similar to Theorem 4.9, we show the consistency of the proposed sample-based barycenter estimator. Let \hat{s}_i be the empirical measure supported over m samples from s_i . From the proof of Lemma 4.11 and 21, recall that,

$$\mathcal{B}'_m(s_1, \dots, s_n) = \min_{\alpha_1, \dots, \alpha_n \geq 0} \sum_{i=1}^n \rho_i \left(\text{Tr}(\alpha_i \mathcal{C}_i^\top) + \lambda_1 \|\alpha_i \mathbf{1} - \hat{s}_i\|_{G_{ii}}^2 + \lambda_2 \|\alpha_i^\top \mathbf{1} - \sum_{j=1}^n \rho_j \alpha_j^\top \mathbf{1}\|_G^2 \right).$$

Theorem B3. Let $\mathcal{B}(s_1, \dots, s_n) \equiv \min_{\beta \geq 0} \sum_{i=1}^n \rho_i \mathcal{U}(s_i, \beta)$ where $\mathcal{U}(s_i, \beta) \equiv \min_{\pi^i \geq 0} \int c \, d\pi^i + \lambda_1 \text{MMD}^2(\pi_1^i, s_i) + \lambda_2 \text{MMD}^2(\pi_2^i, \beta)$. Let π^{i*} be the solution of $\mathcal{U}(s_i, \beta)$. Let $\eta^i(x, z) \equiv \frac{\pi^{i*}(x, z)}{s_i(x)\beta(z)}$, $\eta_1^i(x) \equiv \frac{\pi_1^{i*}(x)}{s_0(x)}$ and $\eta_2^i(x) \equiv \frac{\pi_2^{i*}(x)}{\beta(z)}$. Under mild assumptions that the functions, $\eta^i, \eta_1^i, \eta_2^i$ and $c \in \mathcal{H}_k$, we have that w.h.p., the estimation error, $|\mathcal{B}'_m(\hat{s}_1, \dots, \hat{s}_m) - \mathcal{B}(s_1, \dots, s_n)| \leq \mathcal{O}(m^{-1/2})$.

³Analogous derivations can be done with any other such finite parameterizations too.

Proof. From triangle inequality,

$$|\mathcal{B}'_m(\hat{s}_1, \dots, \hat{s}_n) - \mathcal{B}(s_1, \dots, s_n)| \leq |\mathcal{B}'_m(\hat{s}_1, \dots, \hat{s}_n) - \mathcal{B}'_m(s_1, \dots, s_n)| + |\mathcal{B}'_m(s_1, \dots, s_n) - \mathcal{B}(s_1, \dots, s_n)|, \quad (22)$$

where $\mathcal{B}'_m(s_1, \dots, s_n)$ is same as $\mathcal{B}(s_1, \dots, s_n)$ except that it employs restricted feasibility sets, $\mathcal{F}_i(\hat{s}_1, \dots, \hat{s}_n)$ for corresponding α_i as the set of all joints supported at the samples in $\hat{s}_1, \dots, \hat{s}_n$ alone. Let $\mathcal{D}_i = \{x_{i1}, \dots, x_{im}\}$ and the union of all samples, $\cup \mathcal{D}_{i=1}^n = \{z_1, \dots, z_{mn}\}$.

$\mathcal{F}_i(\hat{s}_1, \dots, \hat{s}_n) \equiv \left\{ \sum_{l=1}^m \sum_{j=1}^{mn} \alpha_{lj} \delta_{(x_{il}, z_j)} \mid \alpha_{lj} \geq 0 \forall l = 1, \dots, m; j = 1, \dots, mn \right\}$. Here, δ_r is the dirac measure at r . We begin by bounding the first term.

We denote the (common) objective in $\hat{\mathcal{B}}_m(\cdot)$, $\bar{\mathcal{B}}(\cdot)$ as a function of the transport plans, (π^1, \dots, π^n) , by $h(\pi^1, \dots, \pi^n, \cdot)$.

$$\begin{aligned} \mathcal{B}'_m(\hat{s}_1, \dots, \hat{s}_n) - \mathcal{B}'_m(s_1, \dots, s_n) &= \min_{\pi^i \in \mathcal{F}_i(\hat{s}_1, \dots, \hat{s}_n)} h(\pi^1, \dots, \pi^n, \hat{s}_1, \dots, \hat{s}_n) - \\ &\quad \min_{\pi^i \in \mathcal{F}_i(\hat{s}_1, \dots, \hat{s}_n)} h(\pi^1, \dots, \pi^n, s_1, \dots, s_n) \\ &\leq h(\pi^{1*}, \dots, \pi^{n*}, \hat{s}_1, \dots, \hat{s}_n) - h(\pi^{1*}, \dots, \pi^{n*}, s_1, \dots, s_n) \\ &\quad \left(\text{where } \pi^{i*} = \arg \min_{\pi^i \in \mathcal{F}_i(\hat{s}_1, \dots, \hat{s}_n)} h(\pi^1, \dots, \pi^n, s_1, \dots, s_n) \text{ for } i \in [1, n] \right) \\ &= \sum_{i=1}^n \rho_i \left\{ \lambda_1 (\text{MMD}^2(\pi_1^{i*}, \hat{s}_i) - \text{MMD}^2(\pi_1^{i*}, s_i)) + \right. \\ &\quad \left. \lambda_2 \left(\text{MMD}^2 \left(\pi_2^{i*}, \sum_{j=1}^n \rho_j \pi_2^{j*} \right) - \text{MMD}^2 \left(\pi_2^{i*}, \sum_{j=1}^n \rho_j \pi_2^{j*} \right) \right) \right\} \\ &= \sum_{i=1}^n \rho_i \lambda_1 (\text{MMD}(\pi_1^{i*}, \hat{s}_i) - \text{MMD}(\pi_1^{i*}, s_i)) (\text{MMD}(\pi_1^{i*}, \hat{s}_i) + \text{MMD}(\pi_1^{i*}, s_i)) \\ &\stackrel{(1)}{\leq} 2\lambda_1 M \sum_{i=1}^n \rho_i (\text{MMD}(\pi_1^{i*}, \hat{s}_i) - \text{MMD}(\pi_1^{i*}, s_i)) \\ &\leq 2\lambda_1 M \sum_{i=1}^n \text{MMD}(\hat{s}_i, s_i) \quad (\text{As MMD satisfies Triangle Inequality}), \end{aligned}$$

where for inequality (1) we use that $\max_{a \in \mathcal{R}_1^+(\mathcal{X})} \max_{b \in \mathcal{R}_1^+(\mathcal{X})} \text{MMD}(a, b) = M < \infty$ as its generating set is compact.

As with probability at least $1 - \delta$, $\text{MMD}(\hat{s}_i, s_i) \leq \frac{1}{\sqrt{m}} + \sqrt{\frac{2 \log(1/\delta)}{m}}$ [61], with union bound, we get that the first term in inequality (22) is upper-bounded by $2\lambda_1 M \left(\frac{1}{\sqrt{m}} + \sqrt{\frac{2 \log n/\delta}{m}} \right)$, with probability at least $1 - \delta$.

We next look at the second term in inequality (22): $|\mathcal{B}'_m(s_1, \dots, s_n) - \mathcal{B}(s_1, \dots, s_n)|$. Let $(\bar{\pi}^1, \dots, \bar{\pi}^n)$ be the solutions of $\mathcal{B}'_m(s_1, \dots, s_n)$. Let $(\pi^{1*}, \dots, \pi^{n*})$ be the solutions of $\mathcal{B}(s_1, \dots, s_n)$. Consider the transport plans:

$\hat{\pi}^{im} \in \mathcal{F}_i(\hat{s}_1, \dots, \hat{s}_n)$ such that $\hat{\pi}^{im}(l, j) = \frac{n_{lj}^i}{m^{2n}}$ where $\eta_{lj}^i = \frac{\pi^{i*}(X_l, Z_j)}{s_i(X_l)\beta(Z_j)}$ for $l \in [1, m]; j \in [1, mn]$.

$$\begin{aligned}
|\mathcal{B}'_m(s_1, \dots, s_n) - \mathcal{B}(s_1, \dots, s_n)| &= \mathcal{B}'_m(s_1, \dots, s_n) - \mathcal{B}(s_1, \dots, s_n) \\
&= h(\bar{\pi}^{1m}, \dots, \bar{\pi}^{nm}, s_1, \dots, s_n) - h(\pi^{1*}, \dots, \pi^{n*}, s_1, \dots, s_n) \\
&\leq h(\hat{\pi}^{1m}, \dots, \hat{\pi}^{nm}, s_1, \dots, s_n) - h(\pi^{1*}, \dots, \pi^{n*}, s_1, \dots, s_n) \\
&\leq \sum_{i=1}^n \rho_i \left\{ \langle \mu_k(\hat{\pi}^{im}) - \mu_k(\pi^{i*}), c_i \rangle + 2\lambda_1 M \|\mu_k(\hat{\pi}_1^{im}) - \mu_k(\pi_1^{i*})\|_{\mathcal{H}_k} + \right. \\
&\quad \left. 2\lambda_2 M \left(\|\mu_k(\hat{\pi}_2^{im}) - \mu_k(\sum_{j=1}^n \rho_j \hat{\pi}_2^{jm})\|_{\mathcal{H}_k} - \|\mu_k(\pi_2^{i*}) - \mu_k(\sum_{j=1}^n \rho_j \pi_2^{j*})\|_{\mathcal{H}_k} \right) \right\} \\
&\quad \text{(Upper-bounding the sum of two MMD terms by } 2M) \\
&\leq \sum_{i=1}^n \rho_i \left\{ \langle \mu_k(\hat{\pi}^{im}) - \mu_k(\pi^{i*}), c_i \rangle + 2\lambda_1 M \|\mu_k(\hat{\pi}_1^{im}) - \mu_k(\pi_1^{i*})\|_{\mathcal{H}_k} + \right. \\
&\quad \left. 2\lambda_2 M \left(\|\mu_k(\hat{\pi}_2^{im}) - \mu_k(\pi_2^{i*})\|_{\mathcal{H}_k} + \sum_{j=1}^n \rho_j \|\mu_k(\hat{\pi}_2^{jm}) - \mu_k(\pi_2^{j*})\|_{\mathcal{H}_k} \right) \right\} \\
&\quad \text{(Triangle Inequality and linearity of the kernel mean embedding)} \\
&\leq \sum_{i=1}^n \rho_i \left\{ \|\mu_k(\hat{\pi}^{im}) - \mu_k(\pi^{i*})\|_{\mathcal{H}_k} \|c_i\|_{\mathcal{H}_k} + 2\lambda_1 M \|\mu_k(\hat{\pi}_1^{im}) - \mu_k(\pi_1^{i*})\|_{\mathcal{H}_k} + \right. \\
&\quad \left. 2\lambda_2 M \left(\|\mu_k(\hat{\pi}_2^{im}) - \mu_k(\pi_2^{i*})\|_{\mathcal{H}_k} + \sum_{j=1}^n \rho_j \|\mu_k(\hat{\pi}_2^{jm}) - \mu_k(\pi_2^{j*})\|_{\mathcal{H}_k} \right) \right\} \\
&\quad \text{(Holder's Inequality)}
\end{aligned}$$

Proceeding the same way as in B.12 (for bounding the second term in the proof of Theorem 4.9), we get that

$$\begin{aligned}
\|\mu_k(\hat{\pi}^{im}) - \mu_k(\pi^{i*})\|_{\mathcal{H}_k} &\leq \|\eta^i\|_{\mathcal{H}_k} \|\mu_k(\hat{s}_i) \otimes \mu_k(\beta) - \mu_k(s_i) \otimes \mu_k(\beta)\| \\
&= \|\eta^i\|_{\mathcal{H}_k} \|(\mu_k(\hat{s}_i) - \mu_k(s_i)) \otimes \mu_k(\beta)\| \\
&= \|\eta^i\|_{\mathcal{H}_k} \|(\mu_k(\hat{s}_i) - \mu_k(s_i))\| \|\mu_k(\beta)\| \\
&\leq \|\eta^i\|_{\mathcal{H}_k} \|(\mu_k(\hat{s}_i) - \mu_k(s_i))\| \quad \text{(With a normalized kernel).}
\end{aligned}$$

From the union bound, with probability at least $1 - \delta$, $|\mathcal{B}'_m(s_1, \dots, s_n) - \mathcal{B}(s_1, \dots, s_n)| \leq \frac{1}{\sqrt{m}} \left(\sum_{i=1}^n \rho_i \left(\|\eta^i\|_{\mathcal{H}_k} \|c_i\|_{\mathcal{H}_k} + 2\lambda_1 M \|\eta_1^i\|_{\mathcal{H}_k} + 2\lambda_2 M \left(\|\eta_2^i\|_{\mathcal{H}_k} + \sum_{j=1}^n \rho_j \|\eta_2^j\|_{\mathcal{H}_k} \right) \right) \right) (1 + \sqrt{2 \log n(3+n)/\delta})$.

Again, applying union bound, for combining the two terms in 22, we that with probability at least $1 - \delta$, the estimation error, $|\mathcal{B}'_m(\hat{s}_1, \dots, \hat{s}_n) - \mathcal{B}(s_1, \dots, s_n)| \leq \frac{1}{\sqrt{m}} \left(\sum_{i=1}^n \rho_i \left(\|\eta^i\|_{\mathcal{H}_k} \|c_i\|_{\mathcal{H}_k} + 2\lambda_1 M \|\eta_1^i\|_{\mathcal{H}_k} + 2\lambda_2 M \|\eta_2^i\|_{\mathcal{H}_k} + \sum_{j=1}^n \rho_j \|\eta_2^j\|_{\mathcal{H}_k} \right) + 2\lambda_1 M n \right) (1 + \sqrt{2 \log n(4+n)/\delta})$. \square

B.16 More on Formulation (9)

Analogous to Formulation (9) in the main paper, we consider the following formulation where an IPM raised to the q^{th} power with $q > 1 \in \mathbb{Z}$ is used for regularization.

$$U_{\mathcal{G}, c, \lambda_1, \lambda_2, q}(s_0, t_0) \equiv \min_{\pi \in \mathcal{R}^+(\mathcal{X} \times \mathcal{X})} \int c \, d\pi + \lambda_1 \gamma_{\mathcal{G}}^q(\pi_1, s_0) + \lambda_2 \gamma_{\mathcal{G}}^q(\pi_2, t_0) \quad (23)$$

Formulation (9) in the main paper is a special case of Formulation (23), when IPM is MMD and $q = 2$.

Following the proof in Lemma B1, one can easily show that

$$U_{\mathcal{G}, c, \lambda_1, \lambda_2, q}(s_0, t_0) \equiv \min_{s, t \in \mathcal{R}^+(\mathcal{X})} |s| W_1(s, t) + \lambda_1 \gamma_{\mathcal{G}}^q(s, s_0) + \lambda_2 \gamma_{\mathcal{G}}^q(t, t_0). \quad (24)$$

To simplify notations, we denote $U_{\mathcal{G},c,\lambda,\lambda,2}$ by U in the following. It is easy to see that U satisfies the following properties by inheritance.

1. $U \geq 0$ as each of the terms in the objective in Formulation (24) is greater than 0.
2. $U(s_0, t_0) = 0 \iff s_0 = t_0$, whenever the IPM used for regularization is a norm-induced metric. As $W_1, \gamma_{\mathcal{G}}$ are non-negative terms, $U(s_0, t_0) = 0 \iff s = t, \gamma_{\mathcal{G}}(s, s_0) = 0, \gamma_{\mathcal{G}}(t, t_0) = 0$. If IPM used for regularization is a norm-induced metric, the above condition reduces to $s_0 = t_0$.
3. $U(s_0, t_0) = U(t_0, s_0)$ as each term in Formulation (24) is symmetric.

We now derive sample complexity with Formulation (23).

Lemma S.4. *Let us denote $U_{\mathcal{G},c,\lambda_1,\lambda_2,q}$ defined in Formulation (8) by U , where $q > 1 \in \mathbb{Z}$. Let \hat{s}_m, \hat{t}_m denote the empirical estimates of $s_0, t_0 \in \mathcal{R}_1^+(\mathcal{X})$ respectively with m samples. Then, $U(\hat{s}_m, \hat{t}_m) \rightarrow U(s_0, t_0)$ at a rate same as that of $\gamma_{\mathcal{G}}(\hat{s}_m, s_0) \rightarrow 0$.*

Proof.

$$U(s_0, t_0) \equiv \min_{\pi \in \mathcal{R}^+(\mathcal{X} \times \mathcal{X})} h(\pi, s_0, t_0) \equiv \int c \, d\pi + \lambda \gamma_{\mathcal{G}}^q(\pi_1, s_0) + \lambda \gamma_{\mathcal{G}}^q(\pi_2, t_0)$$

We have,

$$\begin{aligned} U(s_m, t_m) - U(s_0, t_0) &= \min_{\pi \in \mathcal{R}^+(\mathcal{X} \times \mathcal{X})} h(\pi, \hat{s}_m, \hat{t}_m) - \min_{\pi \in \mathcal{R}^+(\mathcal{X} \times \mathcal{X})} h(\pi, s_0, t_0) \\ &\leq h(\pi^*, \hat{s}_m, \hat{t}_m) - h(\pi^*, s_0, t_0) \left(\text{where } \pi^* = \arg \min_{\pi \in \mathcal{R}^+(\mathcal{X} \times \mathcal{X})} h(\pi, s_0, t_0) \right) \\ &= \lambda (\gamma_{\mathcal{G}}^q(\pi_1^*, \hat{s}_m) - \gamma_{\mathcal{G}}^q(\pi_1^*, s_0) + \gamma_{\mathcal{G}}^q(\pi_2^*, \hat{t}_m) - \gamma_{\mathcal{G}}^q(\pi_2^*, t_0)) \\ &= \lambda \left((\gamma_{\mathcal{G}}(\pi_1^*, \hat{s}_m) - \gamma_{\mathcal{G}}(\pi_1^*, s_0)) \left(\sum_{i=0}^{q-1} \gamma_{\mathcal{G}}^i(\pi_1^*, \hat{s}_m) \gamma_{\mathcal{G}}^{q-1-i}(\pi_1^*, s_0) \right) \right) + \\ &\quad \lambda \left((\gamma_{\mathcal{G}}(\pi_2^*, \hat{t}_m) - \gamma_{\mathcal{G}}(\pi_2^*, t_0)) \left(\sum_{i=0}^{q-1} \gamma_{\mathcal{G}}^i(\pi_2^*, \hat{t}_m) \gamma_{\mathcal{G}}^{q-1-i}(\pi_2^*, t_0) \right) \right) \\ &\leq \lambda \left(\gamma_{\mathcal{G}}(s_0, \hat{s}_m) \left(\sum_{i=0}^{q-1} \gamma_{\mathcal{G}}^i(\pi_1^*, \hat{s}_m) \gamma_{\mathcal{G}}^{q-1-i}(\pi_1^*, s_0) \right) \right) + \\ &\quad \lambda \left(\gamma_{\mathcal{G}}(t_0, \hat{t}_m) \left(\sum_{i=0}^{q-1} \gamma_{\mathcal{G}}^i(\pi_2^*, \hat{t}_m) \gamma_{\mathcal{G}}^{q-1-i}(\pi_2^*, t_0) \right) \right) \quad (\because \gamma_{\mathcal{G}} \text{ satisfies triangle inequality}) \\ &\leq \lambda \left(\gamma_{\mathcal{G}}(s_0, \hat{s}_m) \sum_{i=0}^{q-1} \left(\binom{q-1}{i} \gamma_{\mathcal{G}}^i(\pi_1^*, \hat{s}_m) \gamma_{\mathcal{G}}^{q-1-i}(\pi_1^*, s_0) \right) \right) + \\ &\quad \lambda \left(\gamma_{\mathcal{G}}(t_0, \hat{t}_m) \left(\sum_{i=0}^{q-1} \binom{q-1}{i} \gamma_{\mathcal{G}}^i(\pi_2^*, \hat{t}_m) \gamma_{\mathcal{G}}^{q-1-i}(\pi_2^*, t_0) \right) \right) \\ &= \lambda \left(\gamma_{\mathcal{G}}(s_0, \hat{s}_m) (\gamma_{\mathcal{G}}(\pi_1^*, \hat{s}_m) + \gamma_{\mathcal{G}}(\pi_1^*, s_0))^{q-1} \right. \\ &\quad \left. + \gamma_{\mathcal{G}}(t_0, \hat{t}_m) (\gamma_{\mathcal{G}}(\pi_2^*, \hat{t}_m) + \gamma_{\mathcal{G}}(\pi_2^*, t_0))^{q-1} \right) \\ &\leq \lambda (2M)^{q-1} (\gamma_{\mathcal{G}}(s_0, \hat{s}_m) + \gamma_{\mathcal{G}}(t_0, \hat{t}_m)). \end{aligned}$$

For the last inequality, we use that $\max_{a \in \mathcal{R}_1^+(\mathcal{X})} \max_{b \in \mathcal{R}_1^+(\mathcal{X})} \gamma_{\mathcal{G}}(a, b) = M < \infty$ as the domain is compact.

Similarly, one can show the other way inequality, resulting in the following.

$$|U(s_0, t_0) - U(s_m, t_m)| \leq \lambda (2M)^{q-1} (\gamma_{\mathcal{G}}(s_0, \hat{s}_m) + \gamma_{\mathcal{G}}(t_0, \hat{t}_m)). \quad (25)$$

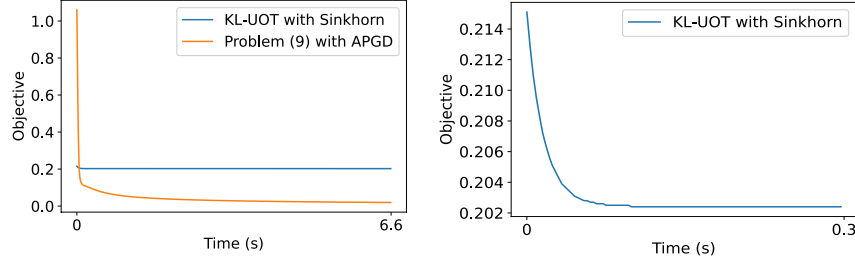


Figure 2: Computation time: Convergence plots with $m = 5000$ for the case of the same source and target measures where the optimal objective is expected to be 0. Left: MMD-UOT Problem (9) solved with accelerated projected gradient descent. Right: ϵ KL-UOT’s convergence plot is shown separately. We observe that ϵ KL-UOT’s objective plateaus in 0.3 seconds. We note that our convergence to the optimal objective is faster than that of ϵ KL-UOT.

The rate at which $|U(s_m, t_m) - U(s_0, t_0)|$ goes to zero is hence the same as that with which either of the IPM terms goes to zero. For example, if the IPM used for regularization is MMD with a normalized kernel, then $\text{MMD}(s_0, \hat{s}_m) \leq \sqrt{\frac{1}{m}} + \sqrt{\frac{2 \log(1/\delta)}{m}}$ with probability at least $1 - \delta$ [61].

From the union bound, with probability at least $1 - \delta$, $|U(s_m, t_m) - U(s_0, t_0)| \leq 2\lambda(2M)^{q-1} \left(\sqrt{\frac{1}{m}} + \sqrt{\frac{2 \log(2/\delta)}{m}} \right)$.

Thus, $O\left(\frac{1}{\sqrt{m}}\right)$ is the common bound for the rate at which the LHS as well as the $\text{MMD}(s_0, \hat{s}_m)$ decays to zero. \square

C Experimental Details and Additional Results

We present more experimental details and additional results in this section. We have followed standard practices to ensure reproducibility. We will open-source the codes to reproduce all our experiments upon acceptance of the paper.

C.1 Synthetic Experiments

Computation Time In Figure (2), we consider the source and target measures to be the same, in which case the optimal objective is 0, and present the Objective vs Time plot. MMD-UOT Problem (9) solved using APGD (described in Section 4.2) gives a much faster rate of decrease in objective compared to the Sinkhorn algorithm used for solving KL-UOT.

The source and target measures are Uniform distributions from which we sample 5000 points. The dimensionality of the data is 5. The experiment is done with hyper-parameters as squared-Euclidean distance, squared-MMD regularization with RBF kernel, sigma as 1 and lambda as 0.1. ϵ KL-UOT’s entropic regularization coefficient is 0.01, and lambda is 1. We choose entropic regularization coefficient from the set $\{1e-3, 1e-2, 1e-1\}$ and lambda from the set $\{1e-2, 1e-1, 1\}$. This hyper-parameter resulted in the fastest convergence. This experiment was done on an NVIDIA-RTX 2080 GPU.

Transport Plan and Barycenter We perform synthetic experiments with the source and target as Gaussian measures. We compare the OT plan of ϵ KL-UOT and MMD-UOT in Figure 3(a). We observe that the MMD-UOT plan is sparser compared to the ϵ KL-UOT plan. In Figure 3(b), we visualize the barycenter interpolating between the source and target, obtained with MMD, ϵ KL-UOT and MMD-UOT. While MMD barycenter is an empirical average of the measures and hence has two modes, the geometry of measures is considered in both ϵ KL-UOT and MMD-UOT formulations. Barycenters obtained by these methods have the same number of modes (one) as in the source and the target. Moreover, they appear to smoothly approximate the barycenter obtained with OT (solved using a linear program).

We use squared-Euclidean cost as the ground metric. We take points $[1, 2, \dots, 50]$ and consider Gaussian distribution over them with mean, standard deviation as (15, 5) and (35, 3) respectively. The hyperparameters for MMD-UOT are λ as 100 and σ^2 in the RBF kernel ($k(x, y) = \exp\left(\frac{-\|x-y\|^2}{2\sigma^2}\right)$) as 1. The hyperparameters for ϵ KL-UOT are λ and ϵ as 1.

For the barycenter experiment, we take points $[1, 2, \dots, 100]$ and consider Gaussian distribution over them with mean, standard deviation as (20, 5) and (60, 8), respectively. The hyperparameters for MMD-UOT are λ as 100 and σ^2 in the RBF kernel as 10. The hyperparameters for ϵ KL-UOT are λ as 100 and ϵ as 10^{-3} .

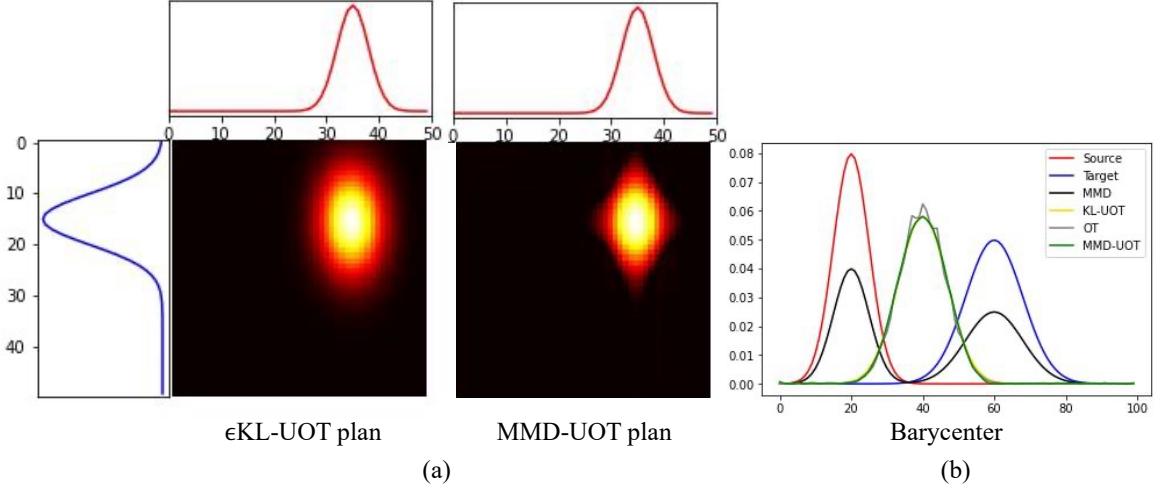


Figure 3: (Best viewed in color) (a) Optimal Transport plans of ϵ KL-UOT and MMD-UOT. (b) Barycenter interpolating between Gaussian measures. For the chosen hyperparameter, the barycenters of ϵ KL-UOT and MMD-UOT overlap and can be looked as smooth approximations of the OT barycenter.

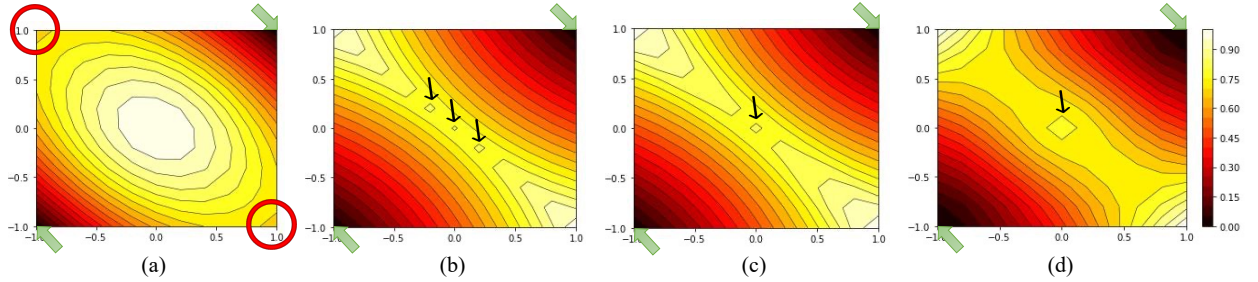


Figure 4: (Best viewed in color) Level sets of distance function between a family of source distributions and a fixed target distribution with the task of finding the source distribution closest to the target distribution using (a) MMD, (b) \bar{W}_2 , (c) ϵ KL-UOT, and (d) MMD-UOT. While all methods correctly identify global minima (green arrows), level sets with MMD-UOT and ϵ KL-UOT show no local minima (encircled in red for MMD) and have a lesser number of non-optimal stationary points (marked with black arrows) compared to (b).

Level set of distances between distributions. Applications like generative modeling deal with optimization over parameter (θ) of the source distribution to match the target distribution. In such cases, it is desirable that the level sets of the distance function over the measures show a lesser number of stationary points which are not global optima [10]. Similar to [10], we consider a model family for source distributions as $\mathcal{F} = \{P_\theta = \frac{1}{2}(\delta_\theta + \delta_{-\theta}) : \theta \in [-1, 1] \times [-1, 1]\}$ and a fixed target distribution Q as $P_{(2,2)} \notin \mathcal{F}$. We compute the distance between P_θ and Q (based on different metrics) and vary θ .

For all OT variants squared-Euclidean is used as a ground metric. For the level set with MMD, RBF kernel is used with σ^2 as 3. For MMD-UOT, λ is 1 and RBF kernel is used with σ^2 as 1. For plotting the level set contours, 20 lines are used for all methods.

Figure 4 presents level sets showing the set of distances $\{d(P_\theta, Q) : \theta \in [-1, 1] \times [-1, 1]\}$ where the distance $d(\cdot, \cdot)$ is measured using MMD, Kantorovich metric, ϵ -KL-UOT, and MMD-UOT (9), respectively. While all methods correctly identify global minima (encircled in green), level sets with MMD-UOT and ϵ KL-UOT show no local minima (encircled in red for MMD) and have a lesser number of non-optimal stationary points (marked with black arrows) compared to the Kantorovich metric in Figure 4(b).

Sample Complexity In Theorem 4.9 in the main paper, we proved an attractive sample complexity of $\mathcal{O}(m^{-\frac{1}{2}})$ for our sample-based estimators. In this section, we present a synthetic experiment to show that the convergence of

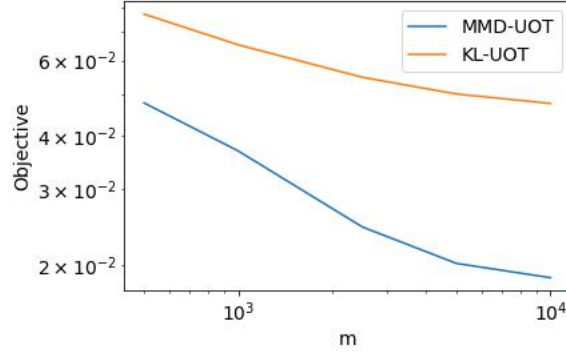


Figure 5: Sample efficiency: Log-log plot of optimal objective vs number of samples. The optimal objective values of MMD-UOT and ϵ KL-UOT formulation are shown as the number of samples increases. The data lies in 10 dimensions, and the source and target measures are both Uniform. MMD-UOT can be seen to have a better rate of convergence.

MMD-UOT’s metric towards the true value is faster than that of ϵ KL-UOT. We sample 10-dimensional sources and target samples from Uniform sources and target marginals, respectively. As the marginals are equal, the metrics over measures should converge to 0 as the number of samples increases. We repeat the experiment with an increasing number of samples. We use squared-Euclidean cost. For ϵ KL-UOT, $\lambda = 1$, $\epsilon = 1e - 2$. For MMD-UOT, $\lambda = 1$ and RBF kernel with $\sigma = 1$ is used. In Figure 5, we plot MMD-UOT’s objective and the square root of the ϵ KL-UOT objective on increasing the number of samples. It can be seen from the plot that the MMD-UOT achieves a better rate of convergence compared to ϵ KL-UOT.

Effect of Regularization In Figures 7 and 6, we visualize matching the marginals of MMD-UOT’s optimal transport plan. We show the results with both RBF kernel $k(x, y) = \exp\left(\frac{-\|x-y\|^2}{2 \cdot 10^{-6}}\right)$ and the IMQ kernel $k(x, y) = (10^{-6} + \|x - y\|^2)^{-0.5}$. As we increase λ , the matching becomes better for unbalanced measures, and the marginals exactly match the given measures in the balanced case. We have also shown the unbalanced case results with KL-UOT. As the POT library [24] doesn’t allow including a simplex constraint for KL-UOT, we do not show this.

C.2 Two-sample Test

Following [41], we repeat the experiment 10 times, and in each trial, we randomly sample a validation subset and a test subset of size N from the given real and fake MNIST datasets. We run the two-sample test experiment for type-II error on the test set for a given trial using the hyperparameters chosen for that trial. The hyperparameters were tuned for $N = 100$ for each trial. The hyperparameters for a given trial were chosen based on the average empirical test power (higher is better) over that trial’s validation dataset.

We use squared-Euclidean distance for MMD-UOT and ϵ KL-UOT formulations. RBF kernel, $k(x, y) = \exp\left(\frac{-\|x-y\|^2}{2\sigma^2}\right)$, is used for MMD and for MMD-UOT formulation. The hyperparameters are chosen from the following set. For the MMD-UOT and MMD, σ was chosen from {median, 40, 60, 80, 100} where the median is the median-heuristic [30]. For the MMD-UOT and ϵ KL-UOT, λ is chosen from {0.1, 1, 10}. For ϵ KL-UOT, ϵ was chosen from {1, 10^{-1} , 10^{-2} , 10^{-3} , 10^{-4} }. Based on validation, σ as the median is chosen for MMD at all trials. For ϵ KL-UOT, the best hyperparameters (λ, ϵ) are (10, 0.001) for trial number 3, (0.1, 0.1) for trial number 10 and (1, 0.1) for the remaining the 8 trials. For MMD-UOT, the best hyperparameters (λ, σ^2) are (0.1, 60) for trial number 9 and (1, median²) for the remaining 9 trials.

C.3 Single-Cell RNA sequencing

scRNA-seq helps us understand how the expression profile of the cells changes over stages [58]. A population of cells is represented as a measure of the gene expression space, and as they grow/divide/die, and the measure evolves over time. While scRNA-seq records such a measure at a time stamp, it does so by destroying the cells [58]. Thus, it is impossible to monitor how the cell population evolves continuously over time. In fact, only a few measurements at discrete timesteps are generally taken due to the cost involved.

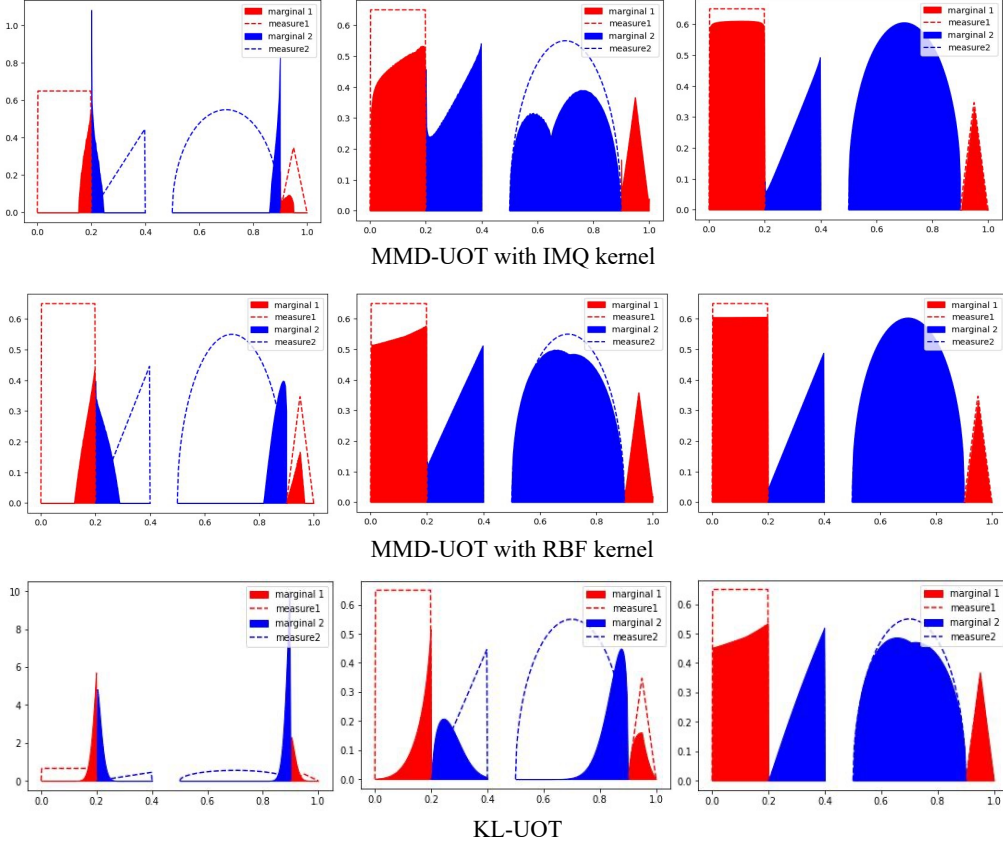


Figure 6: (With unbalanced measures) Visualizing the marginals of transport plans learnt by MMD-UOT (with IMQ and RBF kernels) and KL-UOT, on increasing λ .

Table 6: Additional OT-based baselines for two-sample test: Average Test Power (between 0 and 1; higher is better) on MNIST. MMD-UOT obtains the highest average test power at all timesteps even with the additional baselines.

N	\bar{W}_1	\bar{W}_2	ϵ -OT	MMD-UOT
100	0.111	0.099	0.108	0.154
200	0.232	0.207	0.191	0.333
300	0.339	0.309	0.244	0.588
400	0.482	0.452	0.318	0.762
500	0.596	0.557	0.356	0.873
1000	0.805	0.773	0.508	0.909

The Embryoid Body dataset comprises data at 5 timesteps with sample sizes as 2381, 4163, 3278, 3665 and 3332, respectively.

The MMD barycenter interpolating between measures s_0, t_0 has the closed form solution as $\frac{1}{2}(s_0 + t_0)$. For evaluating the performance at timestep t_i , we select the hyperparameters based on the task of predicting for $\{t_1, t_2, t_3\} \setminus t_i$. We use IMQ kernel $k(x, y) = \left(\frac{1 + \|x - y\|^2}{K^2}\right)^{-0.5}$. The λ hyperparameter for the validation of MMD-UOT is chosen from $\{0.1, 1, 10\}$ and K^2 is chosen from $\{1e - 4, 1e - 3, 1e - 2, 1e - 1, \text{median}\}$, where median denotes the median of $\{0.5\|x - y\|^2 \forall x, y \in \mathcal{D} \text{ s.t. } x \neq y\}$ over the training dataset (\mathcal{D}). The chosen (λ, K^2) for timesteps t_1, t_2, t_3 are (1, 0.1), (1, median) and (1, median), respectively. The λ hyperparameter for the validation of ϵ KL-UOT is chosen from $\{0.1, 1, 10\}$ and ϵ is chosen from $\{1e - 5, 1e - 4, 1e - 3, 1e - 2, 1e - 1\}$. The chosen (λ, ϵ) for timesteps t_1, t_2, t_3 are (10, 0.01), (1, 0.1) and (1, 0.1) respectively. In Table 6, we compare against additional OT-based methods $\bar{W}_1, \bar{W}_2, \epsilon$ -OT.

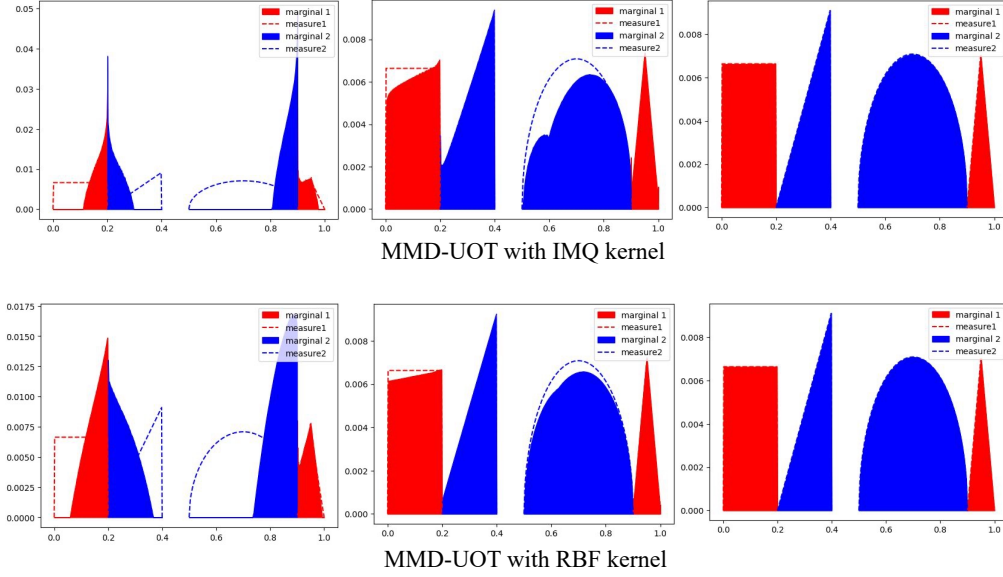


Figure 7: (With balanced measures) Visualizing the marginals of MMD-UOT (solved with simplex constraints) plan on increasing λ .

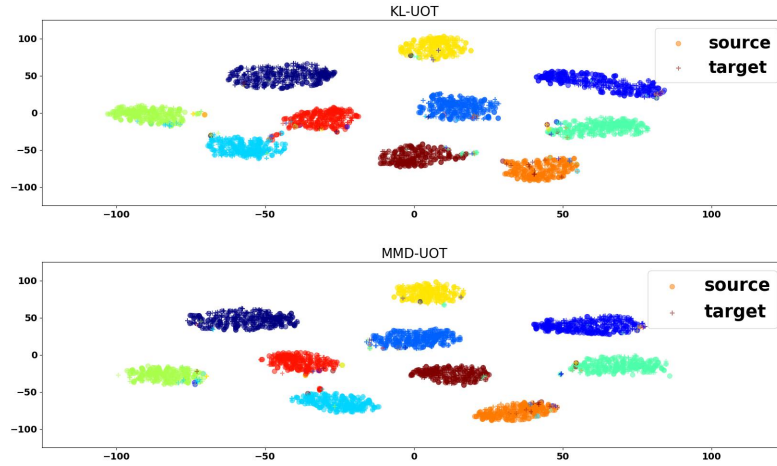


Figure 8: (Best viewed in color) The t-SNE plots of the source and target embeddings learnt for the M-MNIST to USPS domain adaptation task. Different cluster colors imply different classes. The quality of the learnt representations can be judged based on the separation between clusters. The clusters obtained by MMD-UOT seem better separated (for example, the red and the cyan-colored clusters).

C.4 Domain Adaptation in JUMBOT framework

The target accuracies shown in Table 4 in the main paper are computed with the same seed as used by JUMBOT. The chosen hyper-parameters for MMD-UOT are K^2 in the IMQ kernel $k(x, y) = \left(\frac{1 + \|x - y\|^2}{K^2} \right)^{-0.5}$ as 10^{-2} and λ as 100. In Figure 8, we also compare the t-SNE plot of the embeddings learnt with the MMD-UOT and ϵ KL-UOT-based loss. The clusters formed with the proposed MMD-UOT seem better separated (for example, the red and the cyan-colored clusters).

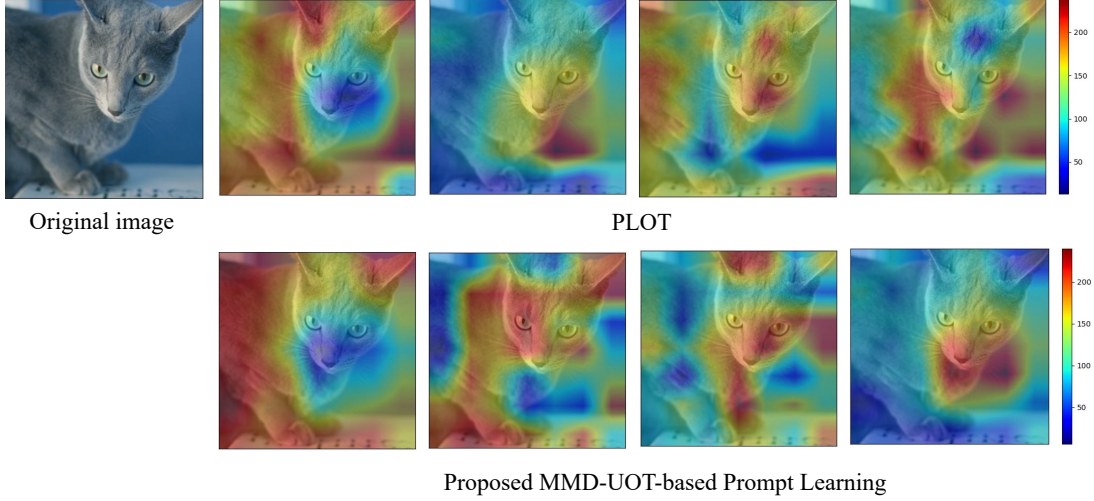


Figure 9: The attention maps corresponding to each of the four prompts for the baseline (PLOT) and the proposed method. The prompts learnt using the proposed MMD-UOT capture diverse attributes for identifying the cat (Oxford-Pets dataset): lower body, upper body, image background and the area near the mouth.

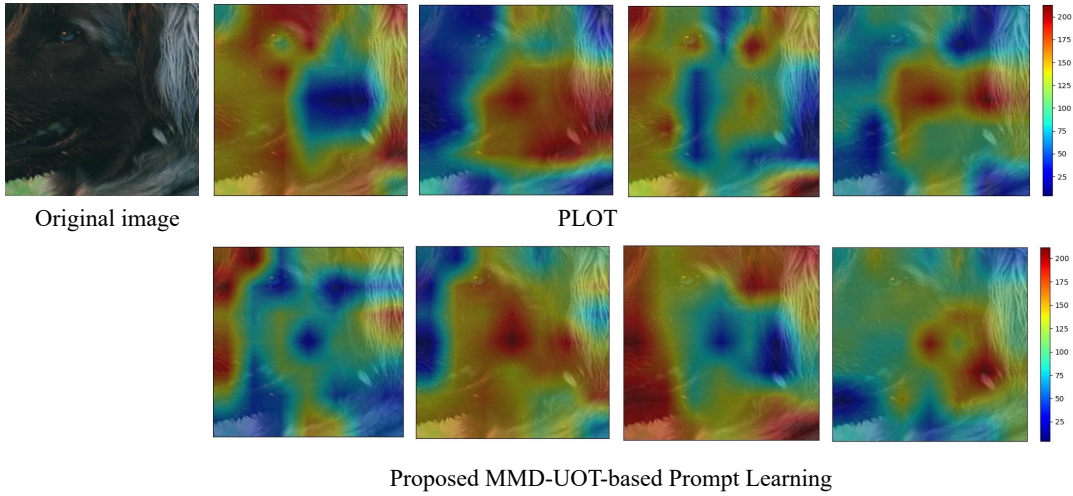


Figure 10: The attention maps corresponding to each of the 4 prompts for the baseline (PLOT) and the proposed method. The prompts learnt using the proposed MMD-UOT capture diverse attributes for identifying the dog (Oxford-Pets dataset): the forehead and the nose, the right portion of the face, the head and the left portion of the face, and the ear.

C.5 Prompt Learning

Let $\mathbf{F} = \{\mathbf{f}_m\}_{m=1}^M$ denote the set of visual features for a given image and $\mathbf{G}_r = \{\mathbf{g}_n\}_{n=1}^N$ denote the set of textual prompt features for class r . Following the setup in the PLOT baseline, an OT distance is computed between empirical measures over 49 image features and 4 textual prompt features, taking cosine similarity cost. Let $d_{OT}(\mathbf{x}, r)$ denote the OT distance between the visual features of image \mathbf{x} and prompt features of class r . The prediction probability is given by $p(y = r|\mathbf{x}) = \frac{\exp((1-d_{OT}(\mathbf{x}, r)/\tau))}{\sum_{r=1}^T \exp((1-d_{OT}(\mathbf{x}, r)/\tau))}$, where T denotes the total no. of classes and τ is the temperature of softmax. The textual prompt embeddings are then optimized with the cross-entropy loss.

Following the PLOT baseline, we use the last-epoch model. The authors empirically found that learning 4 prompts with the PLOT method gave the best results. In our experiments, we keep the number of prompts and the other neural network hyperparameters fixed. We only choose λ and the kernel hyperparameters for prompt learning using MMD-UOT. For this experiment, we also validate over the kernel-type. Besides RBF, we consider two kernels belonging to the IMQ family:

Table 7: Hyperparameters (kernel type, kernel hyperparameter, λ) for the prompt learning experiment.

Dataset	1	2	4	8	16
EuroSAT	(imq2, 10^{-3} , 500)	(imq1, 10^4 , 10^3)	(imq1, 10^{-2} , 500)	(imq1, 10^4 , 500)	(rbf, 1, 500)
DTD	(imq1, 10^{-2} , 10)	(rbf, 100, 100)	(imq2, 10^{-2} , 10)	(rbf, 10^{-2} , 10)	(rbf, 0.1, 1)
Oxford-Pets	(imq2, 0.01, 500)	(rbf, 10^{-3} , 10)	(imq, 1, 10)	(imq1, 0.1, 10)	(imq1, 0.01, 1)

$k(x, y) = \left(\frac{1 + \|x - y\|^2}{K^2}\right)^{-0.5}$ (referred to as imq1) and $k(x, y) = (K^2 + \|x - y\|^2)^{-0.5}$ (referred to as imq2). We choose λ from $\{10, 100, 500, 1000\}$ and kernel hyperparameter (K^2 or σ^2) from $\{1e-3, 1e-2, 1e-1, 1, 10, 1e+2, 1e+3\}$. The chosen hyperparameters are included in Table 7.

C.6 Connections with Spectral Normalized GAN

We comment on the applicability of MMD-UOT in generative modelling and draw connections with the Spectral Norm GAN (SN-GAN) [42] formulation.

A popular approach in generative modelling is to define a parametric function $g_\theta : \mathcal{Z} \mapsto \mathcal{X}$ that takes a noise distribution and generates samples from P_θ distribution. We then learn θ to make P_θ closer to the real distribution, P_r . On formulating this problem with the dual of MMD-UOT derived in Theorem 4.1, we get

$$\min_{\theta} \max_{f \in \mathcal{W}_c \cap \mathcal{G}_k(\lambda)} \int f dP_\theta - \int f dP_r \quad (26)$$

We note that in the above optimization problem, the critic function or the discriminator f should satisfy $\|f\|_c \leq 1$ and $\|f\|_{\mathcal{H}_k} \leq \lambda$ where $\|f\|_c$ denotes the Lipschitz norm under the cost function c . Let the critic function be f_W , parametrized using a deep convolution neural network (CNN) with weights $W = \{W_1, \dots, W_L\}$, where L is the depth of the network. Let \mathcal{F} be the space of all such CNN models, then Problem (26) can be approximated as follows.

$$\min_{\theta} \max_{f_W \in \mathcal{F}; \|f_W\|_c \leq 1, \|f_W\|_{\mathcal{H}_k} \leq \lambda} \int f_W dP_\theta - \int f_W dP_r \quad (27)$$

The constraint $\|f\|_c \leq 1$ is popularly handled using a penalty on the gradient, $\|\nabla f_W\|$ [31]. The constraint on the RKHS norm, $\|f\|_{\mathcal{H}_k}$, is more challenging for an arbitrary neural network. Thus, we follow the approximations proposed in [9]. [9] use the result derived in [8] that constructs a kernel whose RKHS contains a CNN, \bar{f} , with the same architecture and parameters as f but with activations that are smooth approximations of ReLU. With this approximation, [9] show tractable bounds on the RKHS norm. We consider their upper bound based on spectral normalization of the weights in f_W . With this, Problem (27) can be approximated with the following.

$$\min_{\theta} \max_{f_W \in \mathcal{F}} \int f_W dP_\theta - \int f_W dP_r + \rho_1 \|\nabla f_W\| + \rho_2 \sum_{i=1}^L \frac{1}{\lambda} \|W_i\|_{\text{sp}}^2, \quad (28)$$

where $\|\cdot\|_{\text{sp}}$ denotes the spectral norm and $\rho_1, \rho_2 > 0$. Formulations like (28) have been successfully applied as variants of Spectral Normalized GAN (SN-GAN). This shows the utility of MMD-regularized UOT in generative modelling.